Validation and clinical implementation of an MRI-only prostate cancer radiotherapy workflow

Persson, Emilia

2020

Document Version:
Publisher's PDF, also known as Version of record

Validation and Clinical Implementation of an MRI-only Prostate Cancer Radiotherapy Workflow

EMILIA PERSSON
MEDICAL RADIATION PHYSICS | FACULTY OF MEDICINE | LUND UNIVERSITY

Printed by Media-Tryck, Lund 2020 NORDIC SWAN ECOLABEL 3041 0903

LUND UNIVERSITY

FACULTY OF MEDICINE

Department of Translational Medicine
Medical Radiation Physics

Lund University, Faculty of Medicine
Doctoral Dissertation Series 2020:51
ISBN 978-91-7619-912-1
ISSN 1652-8220

Validation and Clinical Implementation of an MRI-only Prostate Cancer Radiotherapy Workflow

Emilia Persson

DOCTORAL DISSERTATION

by due permission of the Faculty of Medicine, Lund University, Sweden.
To be defended in the Lecture Hall, Stora Algatan 4, Lund, on Friday, May 22nd, 2020 at 1:00 p.m.

Faculty opponent
Assistant Professor Neelam Tyagi, Department of Medical Physics,
Memorial Sloan Kettering Cancer Center, New York, USA

Organization LUND UNIVERSITY Medical Radiation Physics Department of Translational Medicine Faculty of Medicine, Lund University	**Document name** DOCTORAL DISSERTATION
	Date of issue May, 22 2020
Author(s) Emilia Persson	Sponsoring organization

Title and subtitle
Validation and clinical implementation of an MRI only prostate cancer radiotherapy workflow

Abstract
The radiotherapy workflow for prostate cancer is associated with systematic uncertainty stemming from the registration between the computed tomography (CT) and magnetic resonance (MR) images. A radiotherapy workflow based solely on MR imaging (MRI), called an MRI-only workflow, has been suggested as a means of eliminating this uncertainty. The aim of the work presented in this thesis was to validate and clinically implement an MRI-only workflow for prostate cancer.

Several aspects of the implementation of an MRI-only workflow have been investigated in the work presented in this thesis. In the registration process between MR and CT images using fiducial markers, the observer bias was found to displace the estimated target position by up to 3 mm, compared to the clinical baseline. The delineated prostate volume was, on average, 18% smaller in the MRI-only delineation procedure than in dual-modality delineation. If this difference is not accounted for, a reduction in the treated volume could arise in the implementation of an MRI-only workflow. Both registration and target delineation uncertainties manifest as systematic deviations for each patient in the dual-modality workflow, which are eliminated in an MRI-only workflow. MRI-only treatment planning employing the synthetic CT (sCT)-generation software MriPlanner™, was validated in a multi-centre/multi-vendor study. The method was found to be robust for a variety of MRI vendors, magnetic field strengths, prescriptions and treatment planning strategies. In the spring of 2017, the first MRI-only-based treatment in Sweden using this software was delivered in a clinical study in Lund. A total of 39 patients were treated in this study using a prospective implementation approach together with an MRI-only workflow. Using a new single-sequence strategy, image registration between different image volumes was eliminated. One patient was excluded due to obesity. CT imaging was included in the workflow for quality assurance (QA) purposes. Acceptance criteria for dose calculations were confirmed within a 2% dose deviation and 98% gamma pass rate. Fiducial marker identification was successfully performed with 100% detection accuracy using MR images. Patient set-up verification was performed, and was within 2 mm of the CT-based set-up verification for most patients.

In the clinical use of an MRI-only workflow there will be no need for CT imaging. An sCT QA method using cone beam CT (CBCT) images was developed to completely remove the need for CT imaging in a clinical MRI-only workflow. CBCT images successfully replaced the CT images in the suggested QA method for sCT images. In conclusion, the work presented in this thesis demonstrates that an MRI-only workflow for radiotherapy of prostate cancer can be clinically implemented.

Key words
radiotherapy, prostate cancer, MRI-only, synthetic CT, implementation, workflow, quality assurance

Classification system and/or index terms (if any)

Supplementary bibliographical information	**Language** English
ISSN and key title 1652-8220 Lund University, Faculty of Medicine Doctoral Dissertation Series 2020:51	**ISBN** 978-91-7619-912-1

Recipient's notes	**Number of pages** 70	Price
	Security classification	

Signature 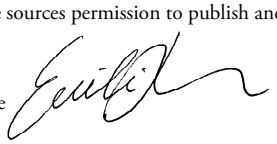 Date 2020-04-17

Validation and Clinical Implementation of an MRI-only Prostate Cancer Radiotherapy Workflow

Emilia Persson

LUND
UNIVERSITY

Medical Radiation Physics
Department of Translational Medicine
Faculty of Medicine, Lund University
Sweden

ISBN 978-91-7619-912-1
ISSN 1652-8220
Lund University, Faculty of Medicine Doctoral Dissertation Series 2020:51

Printed in Sweden by Media-Tryck, Lund University
Lund 2020

To my family –
I love you above all else

"Happiness can be found, even in the darkest of times,
if one only remembers to turn on the light."

Professor Albus Dumbledore
From the movie "Harry Potter and the Prisoner of Azkaban",
based on the book by J K Rowling

Abstract

The radiotherapy workflow for prostate cancer is associated with systematic uncertainty stemming from the registration between the computed tomography (CT) and magnetic resonance (MR) images. A radiotherapy workflow based solely on MR imaging (MRI), called an MRI-only workflow, has been suggested as a means of eliminating this uncertainty. The aim of the work presented in this thesis was to validate and clinically implement an MRI-only workflow for prostate cancer.

Several aspects of the implementation of an MRI-only workflow have been investigated in the work presented in this thesis. In the registration process between MR and CT images using fiducial markers, the observer bias was found to displace the estimated target position by up to 3 mm, compared to the clinical baseline. The delineated prostate volume was, on average, 18% smaller in the MRI-only delineation procedure than in dual-modality delineation. If this difference is not accounted for, a reduction in the treated volume could arise in the implementation of an MRI-only workflow. Both registration and target delineation uncertainties manifest as systematic deviations for each patient in the dual-modality workflow, which are eliminated in an MRI-only workflow. MRI-only treatment planning employing the synthetic CT (sCT)-generation software MriPlanner™, was validated in a multi-centre/multi-vendor study. The method was found to be robust for a variety of MRI vendors, magnetic field strengths, prescriptions and treatment planning strategies. In the spring of 2017, the first MRI-only-based treatment in Sweden using this software was delivered in a clinical study in Lund. A total of 39 patients were treated in this study using a prospective implementation approach together with an MRI-only workflow. Using a new single-sequence strategy, image registration between different image volumes was eliminated. One patient was excluded due to obesity. CT imaging was included in the workflow for quality assurance (QA) purposes. Acceptance criteria for dose calculations were confirmed within a 2% dose deviation and 98% gamma pass rate. Fiducial marker identification was successfully performed with 100% detection accuracy using MR images. Patient set-up verification was performed, and was within 2 mm of the CT-based set-up verification for most patients.

In the clinical use of an MRI-only workflow there will be no need for CT imaging. An sCT QA method using cone beam CT (CBCT) images was developed to completely remove the need for CT imaging in a clinical MRI-only workflow. CBCT images successfully replaced the CT images in the suggested QA method for sCT images. In conclusion, the work presented in this thesis demonstrates that an MRI-only workflow for radiotherapy of prostate cancer can be clinically implemented.

Populärvetenskaplig sammanfattning

Strålbehandling är till för att skada cancerceller, men även friska celler omkring behandlingsområdet riskerar att påverkas. Detta kan leda till biverkningar av olika grad och utsträckning. Urininkontinens och problem med mag- och tarm-kanalen är två biverkningar som kan uppkomma under eller efter strålbehandling av prostatan. För att minska risken för biverkningar är det viktigt att bilderna som används för att bestämma var strålningen ska träffa är av hög kvalitet. I det traditionella arbetsflödet för strålbehandling är det vanligt att magnetresonans (MR)-bilder och bilder från en datortomograf (CT) används. För prostatacancer ger MR-bilder ett utmärkt underlag till att bestämma storlek och läge på prostatan och omkringliggande strålkänsliga organ. CT-bilderna används som underlag för beräkning av hur strålningen fördelas i kroppen, så att rätt dos strålning ges till prostatan medan strålkänsliga organ undviks så mycket som möjligt. Detta arbetsflöde innebär att patienten genomgår två undersökningar inför sin strålbehandling. Detta är inte bara tidskrävande, utan introducerar även ett osäkerhetsmoment då information från MR-bilder måste överföras till CT-bilder.

Syftet med denna avhandling har varit att utveckla och implementera ett nytt arbetsflöde för strålbehandling av prostatacancer där enbart MR-bilder används. Det är värdefullt för både patient och klinik att CT-undersökningen utesluts och ersätts med endast MR-undersökning. Osäkerheter från att använda två bildtekniker försvinner och sjukhuspersonalen får arbeta med de bilder som på bästa sätt visar kroppens anatomi kring bäckenområdet där prostatan finns. Då strålbehandlingssystemen är vana vid att använda CT-bilder i sina beräkningar uppkommer en rad utmaningar när enbart MR-bilder skall användas. Undersökningar av det traditionella arbetsflödet gjordes för att på bästa sätt kunna utveckla det nya arbetsflödet. Vid den traditionella användningen av CT- och MR-bilder i kombination påvisades en osäkerhet i hur bilderna registreras till varandra. Detta riskerade att placera prostatan fel under strålbehandlingen. Vi upptäckte också att onkologer uppskattade att prostatans volym var mindre då CT-bilderna togs bort ut arbetsflödet. En minskning av volymen är positiv, men om den bortses från då det nya arbetsflödet implementeras, riskerar man att oavsiktligt behandla en för liten volym.

MR-bilder kan inte användas för beräkning av strålning utan kräver att bilderna på konstgjord väg omvandlas till att efterlikna CT-bilder, så kallade syntetiska CT-bilder. I en studie där fyra av Sveriges universitetssjukhus medverkade undersöktes en metod för detta. Studien var framgångsrik och visade att syntetiska CT-bilder på ett mycket bra sätt kunde användas för beräkning av strålning. Till följd av denna studie utvecklades ett nytt arbetsflöde för att behandla prostatapatienter vid Skånes Universitetssjukhus i Lund. I en klinisk studie levererades den första behandlingen med

detta nya arbetsflöde i Sverige våren 2017 i Lund. Totalt behandlades 39 av 40 studiepatienter med det nya arbetsflödet. En patient fick uteslutas ur studien på grund av övervikt. En metod för att undersöka kvaliteten på syntetiska CT-bilder utvecklades för att säkerställa att de nya behandlingarna kunde levereras på ett säkert sätt.

Sammanfattningsvis visar arbetena presenterade i denna avhandling att patienter med prostatacancer kan få strålbehandling planerad endast med MR-bilder. Det nya arbetsflödet leder till minskade osäkerheter och har potential att vara tids- och kostnadseffektivt. Arbetena lade grunden till att vi kunde behandla Sveriges första patient med detta arbetsflöde på ett säkert sätt. I framtiden hoppas man att tekniken kommer användas rutinmässigt för strålbehandling av prostatapatienter och leda till en effektivare strålbehandling med mindre biverkningar. Arbete fortgår också med att möjliggöra arbetsflödet för fler diagnoser, exempelvis hjärntumörer.

List of papers

This thesis is based on the research presented in the following papers, which are referred to in the text by their roman numerals. The papers are appended in the end of the thesis.

I. **An investigation of the clinical inter-observer bias in prostate fiducial marker registration of MR and CT images**
Emilia Persson, Sevgi Emin, Jonas Scherman, Christian Jamtheim Gustafsson, Patrik Brynolfsson, Sofie Ceberg, Adalsteinn Gunnlaugsson, Lars E. Olsson
Manuscript

II. **MR-PROTECT: Clinical feasibility of a prostate MRI-only radiotherapy treatment workflow and investigation of acceptance criteria**
Emilia Persson, Christian Jamtheim Gustafsson, Petra Ambolt, Silke Engelholm, Sofie Ceberg, Sven Bäck, Lars E. Olsson, Adalsteinn Gunnlaugsson
Radiation Oncology, 15, 77 (2020)

III. **Target definition in radiotherapy of prostate cancer using magnetic resonance imaging only workflow**
Adalsteinn Gunnlaugsson*, Emilia Persson*, Christian Gustafsson, Elisabeth Kjellén, Petra Ambolt, Silke Engelholm, Per Nilsson and Lars E. Olsson
*Contributed equally to this study
Physics and Imaging in Radiation Oncology, 9, 89-91 (2019)

IV. **MR-OPERA: A multicenter/multivendor validation of magnetic resonance imaging-only prostate treatment planning using synthetic computed tomography images**
Emilia Persson, Christian Gustafsson, Fredrik Nordström, Maja Sohlin, Adalsteinn Gunnlaugsson, Karin Petruson, Nina Rintelä, Kristoffer Hed, Lennart Blomqvist, Björn Zackrisson, Tufve Nyholm, Lars E. Olsson, Carl Siversson, and Joakim Jonsson
International Journal of Radiation Oncology, Biology, Physics, 99(3):692-700 (2017)

V. **Cone beam CT for QA of synthetic CT in MRI only for prostate patients**
Emilia Palmér*, Emilia Persson*, Petra Ambolt, Christian Gustafsson, Adalsteinn Gunnlaugsson, and Lars E. Olsson
*Contributed equally to this study
Journal of Applied Clinical Medical Physics, 19(6):44-52 (2018)

The author's contributions

Paper I	I planned the study, coordinated the observer study and contributed to the data acquisition. I performed the analysis and initial interpretation of the results. I wrote the manuscript.
Paper II	I contributed significantly to the planning of the study and coordinated the clinical work during the implementation of the MRI-only workflow. I performed part of the CT quality control in the study, and contributed to the data acquisition. I contributed significantly to the data analysis and the interpretation of the results. I wrote the paper and was the corresponding author.
Paper III	I contributed significantly to the planning of the study. I contributed to the data acquisition and analysis, and the interpretation of the results. I reviewed and commented on the manuscript.
Paper IV	I contributed significantly to the planning of the study, and coordinated the work in the participating hospitals. I contributed significantly to the data acquisition at one hospital, and the analysis and interpretation of the results. I contributed significantly to the writing of the paper and I was the corresponding author.
Paper V	I contributed significantly to the planning of the study, and contributed to the data acquisition and analysis, and the interpretation of the results. I shared first authorship and I was the corresponding author.

Preliminary reports

Some preliminary reports have also been presented orally at international conferences.

MRI only prostate radiotherapy using synthetic CT-images
Emilia Persson, Fredrik Nordström, Carl Siversson, Crister Ceberg
ESTRO 35, Turin, Italy, 2016

Multi-center/multi-vendor validation of MRI only prostate treatment planning
Emilia Persson, Christian Gustafsson, Fredrik Nordström, Maja Sohlin, Adalsteinn Gunnlaugsson, Karin Petruson, Lennart Blomqvist, Björn Zackrisson, Tufve Nyholm, Lars E. Olsson, Carl Siversson, Joakim Jonsson
4th MRinRT symposium, Ann Arbor, Michigan, USA, 2016

Clinical validation of MR-only prostate treatment planning in a multi-center/multi-vendor environment and patient positioning feasibility using synthetic CT-images
Emilia Persson, Christian Gustafsson, Fredrik Nordström, Maja Sohlin, Adalsteinn Gunnlaugsson, Karin Petruson, Niina Rintelä, Kristoffer Hed, Lennart Blomqvist, Björn Zackrisson, Tufve Nyholm, Lars E. Olsson, Carl Siversson, Joakim Jonsson
5th MRinRT symposium, Sydney, Australia, 2017

Clinical experience from MRI-only radiotherapy – Pearls and pitfalls
Emilia Persson, Petra Ambolt, Christian Gustafsson, Joakim Nilsson, Sven Bäck, Silke Engelholm, Lars E. Olsson, Adalsteinn Gunnlaugsson
6th MRinRT symposium, Utrecht, the Netherlands, 2018

MRI-based treatment planning for prostate cancer
Emilia Persson
ESTRO 38, Milan, Italy, 2019

Other related publications not included in this thesis

Assessment of dosimetric impact of system specific geometric distortion in an MRI only based radiotherapy workflow for prostate
Christian Gustafsson, Fredrik Nordström, Emilia Persson, Johan Brynolfsson, and Lars E. Olsson
Physics in Medicine & Biology, 62(8):2976-89 (2017)

Registration free automatic identification of gold fiducial markers in MRI target delineation images for prostate radiotherapy
Christian Gustafsson, Juha Korhonen, Emilia Persson, Adalsteinn Gunnlaugsson, Tufve Nyholm, and Lars E. Olsson
Medical Physics, 44(11):5563-5574 (2017)

Using C-arm X-ray images from marker insertion to confirm the gold fiducial marker identification in an MRI-only prostate radiotherapy workflow
Christian Gustafsson, Emilia Persson, Adalsteinn Gunnlaugsson, and Lars E. Olsson
Journal of Applied Clinical Medical Physics, 19(6):185-192 (2018)

Abbreviations

CBCT	Cone beam CT
CT	Computed tomography
CTV	Clinical target volume
DVH	Dose volume histogram
DRR	Diagnostic reconstructed radiographs
ED	Electron density
EPID	Electronic portal imaging device
GRE	Gradient echo
HU	Hounsfield unit
LFOV	Large field of view
MEGRE	Multi-echo gradient echo
MR	Magnetic resonance
MRI	Magnetic resonance imaging
OAR	Organs at risk
PET	Positron emission tomography
PTV	Planning target volume
QA	Quality assurance
ROI	Region of interest
sCT	Synthetic CT
SD	Standard deviation
TPS	Treatment planning system
UTE	Ultrashort echo time

Contents

1 Introduction

Magnetic resonance (MR) images are preferred for prostate target delineation due to their superior soft tissue contrast (Salembier et al., 2018). The use of MR images show smaller inter-observer variations (Milosevic et al., 1998, Parker et al., 2003) and smaller target volumes compared to computed tomography (CT) images (Hentschel et al., 2011, Rasch et al., 1999, Seppala et al., 2015, Smith et al., 2007, Tzikas et al., 2011), and play an important role in the radiotherapy workflow for prostate cancer. The advantages of MR imaging (MRI) in radiotherapy have led to solutions facilitating the integration of MRI in radiotherapy. Examples of adaptions advantageous for radiotherapy include flat table tops for patient immobilization in the MR scanner, and bore sizes of 70 cm. This enables identical patient immobilization during MR imaging and treatment. CT images, which provide information in terms of Hounsfield units (HU), are traditionally used for treatment planning, dose calculation and patient set-up. In such dual-modality workflows, image registration is required to relate the CT images to the MR images, which introduces systematic uncertainties (Nyholm et al., 2009).

A number of sources of uncertainty in the radiotherapy workflow have been given by the IAEA (IAEA, 2016). No single value can be used as a measure of the accuracy required in radiotherapy, as it depends on various factors, and varies between hospitals. It is thus recommended that all types of radiotherapy is administered as accurately as reasonably achievable. Recent developments of radiotherapy of prostate cancer involves steeper dose gradients and higher fractionation doses (Widmark et al., 2019), which places higher demands on the accuracy and precision of the delivered dose.

An MRI-only workflow has been suggested as a means of reducing the systematic uncertainties associated with the dual-modality workflow required when using both MR and CT images. As well as offering reduced systematic uncertainties, MRI-only workflows have the potential to be more time- and cost-efficient. However, there are a number of challenges in applying an MRI-only workflow, such as patient immobilization in the MR scanner, geometric uncertainties in MR images and motion during MRI. Estimation of the electron density (ED) from MR images, referred to as synthetic CT (sCT) images, and capability of radiotherapy and MRI are also challenges in the clinical implementation of an MRI-only workflow (Schmidt and Payne, 2015).

In the papers presented in this thesis, several aspects of implementing an MRI-only workflow have been investigated. The observer bias in a commonly used registration approach for MR and CT images, using fiducial markers in the prostate, was investigated (**Paper I**), and the impact on the prostate target delineation process when transitioning from dual-modality to an MRI-only delineation procedure was investigated (**Paper III**). MRI-only treatment planning employing a commercial sCT-generation method (MriPlanner^{TM}), was validated in a multi-centre/multi-vendor study (**Paper IV**). Based on experiences from previous studies (**Papers III** and **IV**), an MRI-only workflow was implemented (**Paper II**). The feasibility of an MRI-only workflow in a clinical setting and the acceptance criteria for future implementations were then investigated. Finally, a sCT quality assurance method using cone beam CT images was investigated (**Paper V**), to completely remove the need for CT images in a future clinical MRI-only prostate radiotherapy workflow.

2 Aims

The overall aim of the work presented in this thesis was to clinically implement an MRI-only workflow for radiotherapy of prostate cancer. To this end, several aspects of an MRI-only prostate cancer radiotherapy workflow were investigated and validated.

The specific goals of each study were:

- to investigate inter-observer image registration bias in the dual-modality workflow (**Paper I**),
- to implement an MRI-only workflow and lay the groundwork for the establishment of acceptance criteria for future implementation (**Paper II**),
- to investigate the impact on the target delineation process when transitioning from a dual-modality to an MRI-only workflow (**Paper III**),
- to validate MRI-only treatment planning using a commercial sCT-generation method (**Paper IV**), and
- to investigate a quality assurance method for sCT images in the clinical use of an MRI-only workflow (**Paper V**).

3 Clinical implementation of an MRI-only workflow

3.1 The motivation

Three major benefits of an MRI-only workflow, which excludes CT imaging, have been identified in literature: 1) time- and cost-efficiency, 2) lower doses of ionizing radiation, and 3) reduced systematic uncertainties (Jonsson et al., 2019).

Time savings of approximately 15 minutes have been reported in the treatment of prostate cancer using an MRI-only workflow as a result of eliminating CT imaging (Tyagi et al., 2017a). Additional time could potentially be saved as delineation of the target is performed directly on the MR images without the need for registration to CT images. However, the introduction of new techniques with increased complexity could lead to an increase in the cost of quality assurance (QA) (IAEA, 2016). This should also be taken into account when performing cost analyses of MRI-only workflows. In a failure mode and effects analysis of the potential implementation of an MRI-only prostate cancer radiotherapy workflow, it was concluded that a QA programme for MRI-only specific tasks was an important risk mitigation tool (Kim et al., 2019).

The dose from a single CT examination is approximately 1-4 cGy within the scanned volume (IAEA, 2016). This can be considered small compared to the total dose delivered to a prostate cancer patient during radiotherapy, which is typically several Gy. Despite being mentioned as an advantage in MRI-only workflows, the advantage to the patient can be questioned. The dose reduction would be of greater importance when adaptive strategies are desired and several imaging sessions are used during the course of treatment. Furthermore, the exclusion of an imaging session could be of great personal value for the patient. Although they are important, and the subject of many interesting discussions, these benefits were not investigated in this thesis.

In the dual-modality workflow, the registration between the CT and MR images may affect the delineation of the treatment volume. Image registration uncertainties have been identified as the main factor contributing to systematic uncertainties in the dual-modality workflow, and were estimated to be 2 mm (Nyholm et al., 2009). Automatic

image registration such as mutual information and marker registration using, for example, fiducial markers, are common approaches for the registration of CT and MR images in the radiotherapy workflow for prostate cancer patients. Several studies have been carried out on image registration methods used in the planning of radiotherapy for prostate cancer. Some of these studies are summarized in Table 1.

Table 1. Studies on various image registration approaches used in planning the treatment of prostate cancer presented in the literature.

Reference	Type of study	No. of patients	Main results
(McLaughlin et al., 2004)	Comparison of automatic MI* registration and seed registration	5	Estimated uncertainty ~2 mm for both methods. Repeated MI registration average random error: 0.3° and 0.7 mm
(Huisman et al., 2005)	Comparison of a landmark- and surface-based method for gold fiducial marker registration	21	Precision better than 2 mm: 86% for surface-based and 42% for landmark-based methods. Time required: 5 min for surface-based and 2 min for landmark-based. Observer dependency included
(Roberson et al., 2005)	Comparison of automatic MI registration and seed registration	12	Registration error ~2 mm for both methods. Time for MI <30 min.
(Vidakovic et al., 2006)	Comparison of automatic MI registration and independent registration	3	Overall MI accuracy (visual assessment): 1.5 mm. Comparable root mean square for the two methods.
(Nyholm et al., 2009)	Literature review	-	Estimated uncertainty in CT-MR image registration: 2.0 mm
(Seppala et al., 2015)	Comparison of gold fiducial marker registration and prostate border registration	30	Average gold seed displacement between gold fiducial marker registration and correction based on the prostate border was 0.5-0.9 mm.
(Korsager et al., 2016)	Comparison of automatic MI registration and landmark registration	30	Dice similarity index: 0.87 (0.77-0.95) Sensitivity: 0.87 (0.74-0.95) Translational and rotational differences: 1.66-1.93 mm (0.00-9.57) and 1.51-3.93° (0.00-14.19)
(Wegener et al., 2019)	Gold fiducial marker registration accuracy measured by two operators	10	Average deviation: 1.9 mm (1.2-2.9)

*MI – mutual information

The point match registration approach in Eclipse™ supplied by Varian Medical Systems (Palo Alto, California, USA), currently in use at Skåne University Hospital for prostate cancer patients, was investigated in the first study (**Paper I**). The image registration routinely created in the clinic was used as the baseline, and the potential observer bias in the approach was investigated. Assuming that the prostate was delineated strictly on the MR images, and then extrapolated to the CT images using the created registrations, a structure misplacement of up to 3 mm was observed compared to the clinical baseline. This observer bias was of the same order of magnitude as image registration uncertainties reported in previous studies (Table 1). In previous studies the method's uncertainty was investigated in a single-mode approach, or between multiple image registration approaches. None of these studies reported the observer bias in comparison to a clinical situation. Manual image registration is commonly used as the baseline for comparison, which is observer dependent. Furthermore, manual image registration often involves a different method from that investigated in the study, for example, when an automatic method is investigated. It is common to use one particular method for the registration of CT and MR images at each clinic. The specific image registration uncertainty at a clinic would thus be better represented by the inter-observer variation in the image registration method used, and not by comparing two methods. However, comparison with another image registration approach is important when a new approach is introduced.

Observer differences are in radiotherapy commonly interpreted as random errors. However, in the case of CT to MR image registration, observer bias becomes a systematic deviation for each patient, since this image registration is only performed once. This systematic uncertainty is related to the imaging, the registration approach and the observer, which has systematic effects on the estimated target position in the CT images. This uncertainty is eliminated in a single-modality workflow. A reduction in the target margin should theoretically be possible in an MRI-only workflow thanks to the superior soft tissue contrast of MRI and the elimination of CT imaging. However, the margin should only be reduced after careful consideration and evaluation of the clinical impact.

The advantages of MRI-only workflows have given rise to a large number of publications on ways in which they can be implemented in radiotherapy clinics. Studies have been published on MRI-based dose calculations, as well as patient set-up strategies (Edmund and Nyholm, 2017, Johnstone et al., 2018), and on the clinical implementation of MRI-only workflows for prostate cancer radiotherapy (Bird et al., 2019).

3.2 Clinical implementations

MRI-only workflows have been clinically implemented at a number of radiotherapy centres around the world (Table 2). The term 'clinical implementation of an MRI-only workflow' in this thesis refers to a workflow that has been developed and used to deliver radiotherapy to one or more patients.

Table 2. Clinical implementation of MRI-only workflows for prostate cancer radiotherapy presented in the literature.

Reference	Type of study	No. of patients treated	Centre
(Christiansen et al., 2017)	Workflow demonstration	1	Odense University Hospital Odense, Denmark
(Tyagi et al., 2017a)	Workflow demonstration	42	Memorial Sloan Kettering Cancer Center New York, USA
(Tenhunen et al., 2018)	Workflow and clinical experience	125	Helsinki University Hospital Helsinki, Finland
(Kerkmeijer et al., 2018)	Workflow demonstration	-	University Medical Center Untecht Utrecht, The Netherlands
(Persson et al., 2018a, Persson et al., 2020)	Prospective study	39	Skåne University Hospital Lund, Sweden
(Greer et al., 2019)	Prospective study, multicentre	25	Calvary Mater Newcastle Hospital Newcastle, Australia Liverpool Hospital Cancer Therapy Centre Sydney, Australia

The implementation of any new workflow must be preceded by evaluation and validation. Dosimetric evaluation and, in some cases, evaluation of the geometric accuracy of MRI and patient set-up strategies have been performed. These evaluations are further discussed in sections 4.1-4.5.

The studies listed in Table 2 include demonstrations of workflows (Christiansen et al., 2017, Tyagi et al., 2017a, Kerkmeijer et al., 2018), as well as clinical experience (Tenhunen et al., 2018) and prospective implementations (Persson et al., 2018a, Greer et al., 2019, Persson et al., 2020). A comparison of early clinical data between an MRI-only cohort and a dual-modality cohort, has also been presented (Tenhunen et al., 2018). In contrast to the workflow demonstrations and clinical experience, we chose to

investigate a prospective implementation approach, where CT imaging was included in the workflow (**Paper II**). The first MRI-only-based treatment in Sweden using this approach was delivered in Lund in the spring of 2017 (Persson et al., 2018a, Persson et al., 2020). The prospective approach was also adopted at another clinic in Australia (Greer et al., 2019).

A widespread implementation of an MRI-only workflow would benefit from recommended acceptance criteria for different parts of the workflow. Greer et al. (2019) verified specific tasks in the workflow, and treatment was delivered only if the acceptance criteria were within specified limits. When comparing the CT and sCT dose distributions, the acceptance criteria of an isocenter dose deviation below 2% and a 2%/2 mm gamma pass rate above 90% were satisfied for all 25 patients in the study. Fiducial marker identification on MR images was within the 1 mm acceptance criterion, compared to the position of the fiducial markers in the CT images. However, these authors did not specify how the acceptance criteria were determined.

In the present work (**Paper II**), a CT examination was included in the workflow to enable validation during implementation and retrospective investigation of the acceptance criteria. This was the first MRI-only workflow to incorporate sCT images generated with the MriPlanner software (Spectronic Medical AB, Helsingborg, Sweden). Fiducial marker identification was achieved with a maximum difference of 2.2 mm compared to the positions in the CT images. Dose differences were below 2% of the prescribed dose, and the 2%/2mm global gamma pass rates were above 98%. The results obtained in this study support the dose deviation acceptance criterion of 2% used by Greer et al. (Greer et al., 2019). The suggested gamma pass rate acceptance criterion of 90% was easily achieved in both prospective studies as all the patients reached a 98% pass rate. Fiducial marker identification is dependent on the method of identification used, as well as the slice thickness, and acceptance criteria should be based on local routines. The study presented in **Paper II** demonstrated the feasibility of excluding CT imaging and implementing an MRI-only prostate cancer radiotherapy workflow.

4 The MRI-only prostate cancer radiotherapy workflow

Sections 4.1-4.5 describe an MRI-only workflow for prostate cancer radiotherapy, in which the CT examination has been excluded. The workflow is illustrated in Figure 1.

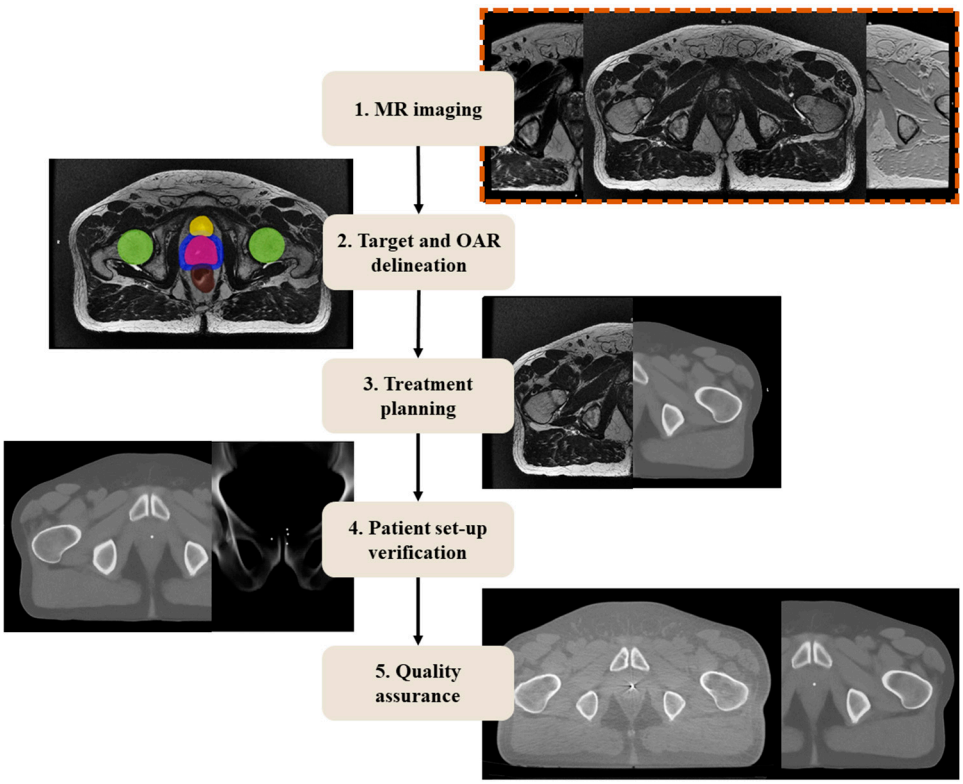

Figure 1. Illustration of the MRI-only workflow described in this thesis. The workflow includes five steps: 1. MR imaging, 2. delineation of the target and organs at risk (OAR), 3. treatment planning, 4. patient set-up verification and 5. quality assurance. This workflow is the result of several studies presented in this thesis, and other studies not included in this thesis.

4.1 MR imaging

In contrast to radiological examinations in which the aim is to establish a diagnosis, the MR images acquired in the planning of radiotherapy are used to determine the extent of the disease to be treated. Based on the determined treatment volume and the organs at risk (OAR), an individual treatment plan is drawn up for each patient. In an MRI-only workflow, MR is the single imaging modality used for treatment planning.

4.1.1 Patient immobilization

The first task is to position the patient correctly in the MR scanner prior to imaging. The positioning of the patient should be performed in a reproducible manner, enabling the same position to be used during treatment at the linear accelerator. Immobilization devices can be used for this purpose, which, for prostate cancer patients, often include feet and knee-supports, a thin mattress and a head support. The primary goal of immobilization is to limit potential patient motion and to reduce positioning errors (Verhey, 1995).

The MR scanner is customized with a flat table top and receiver coil bridges to enable patient immobilization for radiotherapy. The flat table top with indexing enables the use of radiotherapy fixation devices and allows replication of the patient's position at the time of treatment. Coil bridges are used to lift the coils from the surface of the patient, to avoid impact on the body contour. Placing the coils directly on the patient surface increase the signal to noise ratio compared to if coil bridges are used. However, coil bridges are often used to achieve a consistent patient geometry throughout the workflow (Sun et al., 2015). The use of coil bridges can be avoided by using an immobilization mould specific to each patient, enabling placement of the coil directly on the mould surface (Tyagi et al., 2017a). Lightweight flexible coils, such as the AIR™ Coils provided by GE Healthcare (Chicago, Illinois, USA), are another alternative as they should be light enough not to disturb the patients' surface contour.

Skin marks are used to define the image origin during treatment planning, and to align the patient on the treatment couch. These are made on the skin using a pen or tattoo ink to identify the position of the image origin during MR imaging. This is aided by an external laser system. In the MRI-only workflow, these marks must be visible in the MR images, while not introducing artefacts in the MR images. Capsules containing oil or water can be used for this purpose. Commercial products are also available, for example, "PinPoint for image registration 128" (Beekley Medical, Bristol, Connecticut, USA).

4.1.2 The MRI examination protocol

The primary goal of the MRI examination protocol is to produce images for target and OAR delineation, treatment planning, fiducial marker identification and patient set-up verification. To obtain the image information required for these tasks, several MRI sequences are used. An MRI-only MRI examination protocol for prostate cancer patients was developed and tested (**Paper II**). In this MRI examination protocol (shown in Figure 2), all final decisions were made in the geometry of a large field of view (LFOV) MR image, without the use of image registration. Fiducial marker identification and target and OAR delineation were performed in the LFOV MR images, guided by support sequences acquired directly prior to and after the LFOV sequence.

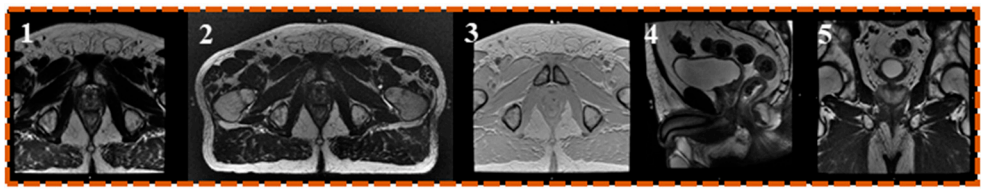

Figure 2. MR images acquired with the MRI examination protocol described in **Paper II**. The images were used for: 1. target delineation support, 2. primary image for target and OAR delineation, treatment planning and fiducial marker identification, 3. fiducial marker identification support, and 4-5. target delineation support.

The LFOV MR images were used for sCT generation in the workflow. To enable sCT generation and dose calculations, the MR images had to cover the body contour of the patient. It was also necessary to include the target area and the relevant OAR. The sequences used for sCT generation in the pelvis are typically a DIXON or a T2 SPACE sequence (Bird et al., 2019). A DIXON sequence acquires images with two different echo times and generates in-phase and out-of-phase images. Water-only and fat-only images are then derived from this single sequence and used for sCT generation (Tyagi et al., 2017b). The preferred images for delineation of the prostate are currently T2-weighted MR images, as stated in the ESTRO SCROP consensus guidelines on CT- and MRI-based target volume delineation for primary radiation therapy of localized prostate cancer (Salembier et al., 2018). It is therefore advantageous to use a T2-weighted MRI sequence for sCT generation, as it allows target and OAR delineation and treatment planning in the same geometry.

Fiducial marker identification has been recognized as one of the greatest challenges in MRI-only workflows (Tenhunen et al., 2018, Tyagi et al., 2017a). Correct and accurate identification of the fiducial markers is important. Fiducial markers are often made of gold, which gives no expected useful nuclear magnetic resonance signal (Zangger and Armitage, 1999), causing them to appear as dark signal voids in MR images. This is a

T2* effect induced by disturbance of the local magnetic field homogeneity by the gold fiducial markers (Schieda et al., 2015). Calcifications and vessels in the prostate have a similar appearance to gold fiducial markers in MR images (Dinis Fernandes et al., 2017, Ghose et al., 2016, Gustafsson et al., 2017a), which may lead to difficulties in distinguishing between the markers and other structures in the prostate. Gradient echo (GRE) sequences, which are sensitive to T2* (Schieda et al., 2015), can be used to increase the sensitivity to susceptibility differences in the image, and improve the visualization of gold fiducial markers in MR images (Port and Pomper, 2000).

The detection accuracy in the manual gold fiducial marker identification method described in **Paper II** was 100%. In this study, a multi-echo gradient echo (MEGRE) sequence (Figure 3) was used to aid the manual determination of the spatial positions of the centre of mass of the gold fiducial markers in the LFOV MR images. The signal void from a gold fiducial marker in the transverse slice is round in the MEGRE images, and the area of the void increases more rapidly with increasing echo time, than the signal from calcifications (Gustafsson et al., 2017a). The positions of the gold fiducial markers in the CT images were considered the true positions and were compared with the positions of the gold fiducial markers identified manually in the MRI-only workflow. The maximum difference between the centroid of the three gold fiducial marker in the CT images and the MR images was 2.2 mm. This difference is roughly the same as the MEGRE image slice thickness, i.e. 2.5 mm. Identification of the gold fiducial markers was restricted to one physical slice of the MR images, and not between the slices. Thus, differences of the same order as the MEGRE image slice thickness were expected, when compared to the CT images.

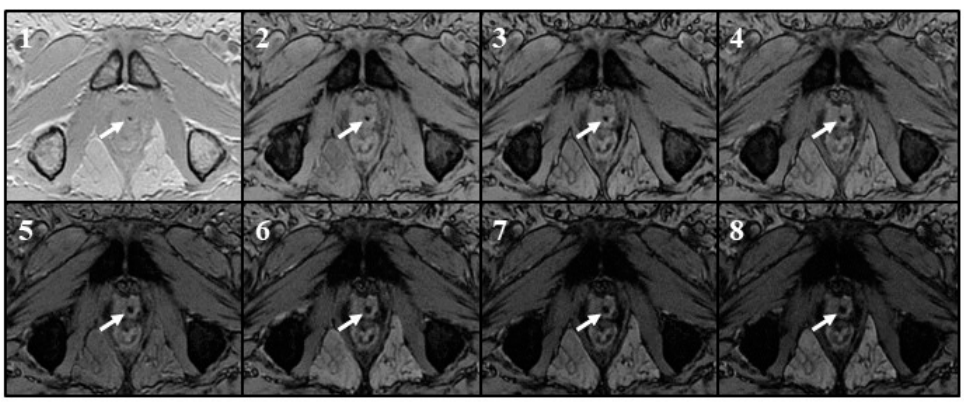

Figure 3. One image slice through the centre of the prostate where a fiducial marker is indicated by the white arrow. The size of the signal void resulting from the fiducial marker increases with increasing echo time. Echoes 1-4 are shown in the first row, from left to right, and echoes 5-8 in the second row, from left to right.

Although manual identification of gold fiducial markers is accurate, it is also time consuming. Automatic methods have therefore been developed to save time and resources, as well as to reduce inter-observer differences (Dinis Fernandes et al., 2017, Ghose et al., 2016, Gustafsson et al., 2017a, Maspero et al., 2017b). However, none of them has yet exhibited 100% detection accuracy, but until such time as they do, they could be useful as efficient decision making tools.

4.1.3 The geometric accuracy of MRI

In order to use MR images in radiotherapy planning, high geometric accuracy in the images is needed. Geometric distortions of MR images can be caused by imperfections in the static magnetic field and the gradient linearity. These distortions are often referred to as system-induced distortions. The patient can also cause distortions, referred to as patient-induced distortions. Patient-induced distortions are caused by the spatial distribution of differences in magnetic susceptibility within the patient, which may disturb the magnetic field (Schmidt and Payne, 2015). This can cause distortions in the shape of the object, which are pronounced in the interface between two materials (Fransson et al., 2001). Both system- and patient-induced geometric distortions are undesirable, especially in images intended for use in radiotherapy planning, and must therefore be minimized.

Geometric distortions can be reduced by using magnetic field shimming (Fransson et al., 2001) and a high acquisition bandwidth (Adjeiwaah et al., 2018). Vendor-specific distortion correction can also be used to correct for gradient non-linearity in two and three dimensions (Wang et al., 2004). In the implementation of MRI-only workflows, it is important to evaluate the potential geometric distortions in the MRI acquisition sequences used for treatment planning and target delineation. Training of staff in the use of MRI will play a significant role in the implementation of MRI-only workflows, and has been identified as important in risk mitigation (Kim et al., 2019). The risk of unintentional changes in MRI parameters can be reduced by training MR technicians. The MRI acquisition parameters can be automatically checked to ensure that they are as specified in the protocol, as described in **Paper II**.

System-specific geometric distortions were evaluated for the sequence used for the sCT generation described in **Papers II**, **IV** and **V** (Gustafsson et al., 2017b). The mean percentage dose difference was less than 0.02% for isodose levels of 0-100%, normalized to 78 Gy. Patient-specific geometric distortions have been reported to result in a relative dose difference of <0.5% in the planning target volume (PTV) (Adjeiwaah et al., 2018). After vendor-specific geometric corrections, the patient-induced distortions were greater than the system-induced distortions. The effects were, however,

small when a high acquisition bandwidth of 488 Hz/pixel was used. Given this, the effects of patient-induced geometric distortions were assumed to be small in the sequence described in **Papers II**, **IV** and **V**, where a bandwidth of 390 Hz/pixel was used.

Lee et al. (2003) investigated radiation treatment planning for prostate cancer and quantified geometric distortions in a FLASH 3D sequence, earlier found to be suitable for prostate delineation. They concluded that the geometric distortions increased with radial distance from the image centre, which will be important when using MRI-only protocols for prostate cancer where LFOV are needed. They found distortions in the prostate volume to be acceptable, since the prostate did not extend far away from the image centre. The impact of geometric distortions on the body outline and OAR should be greater than that on the prostate, due to their position relative to the centre (Lee et al., 2003). This was investigated by our group, and we found that the mean magnitude of geometric distortions of both the prostate and OAR were less than 0.01 mm. The distortions in the body outline were larger, but still less than 0.44 mm (mean) in all directions (Gustafsson et al., 2017b). In conclusion, patient- and system-induced geometric distortions can be assessed in prostate cancer patients, and reduced to a level at which they have negligible dosimetric impact.

4.1.4 Patient-related motion during MRI

Despite the many advantages of MRI, one obvious disadvantage is the significantly longer imaging acquisition time compared to CT imaging. A CT image can be acquired in a few seconds, while several minutes are often required for an MRI examination protocol for prostate cancer patients, during which sequences are acquired for multiple purposes. During this time, there is a risk of movement of the patient and of the internal anatomy of the patient.

Motion of the prostate is well known, and has several different causes (Langen and Jones, 2001). The major causes of prostate motion are rectum activity (Stroom et al., 2000), bladder filling, and patient motion, due either to the movement of external body parts, such as the legs, or internal movements such as muscle clenching (Nederveen et al., 2002). The effect of respiration on prostate motion has been found to be negligible when the patient is in the supine position (Dawson et al., 2000, Nederveen et al., 2002).

The position of the prostate has been shown to drift over time, and changes in the internal anatomy have been reported to affect the prostate location over a short time (Ballhausen et al., 2015). Several studies have reported movement of the prostate over

time, the general consensus being that the longer the duration of treatment, the higher the risk of movement. For treatment durations exceeding 4-6 minutes, repositioning of the patient has been recommended (Cramer et al., 2013). It has also been suggested that limiting the treatment time could be beneficial in reducing uncertainties due to organ motion during hypo-fractionated radiotherapy (Gladwish et al., 2014).

The problems associated with prostate motion have been extensively investigated in relation to radiotherapy treatment delivery, but very little attention has been paid to motion during imaging for treatment planning. This is probably because the image acquisition time is short in CT imaging, which is traditionally used in radiotherapy planning. Motion between sequences in the MRI examination protocol becomes more important in an MRI-only workflow. In a study based on the same MRI examination protocol and patient cohort as described in **Paper II** in this thesis, our group has investigated the motion of the prostate and OAR during MRI (Persson et al., 2018b). Two LFOV MRI sequences were obtained, separated by approximately 30 minutes, while the patient was resting in the MR scanner. Deformable image registration was also used to investigate the variation in internal anatomy during the 30 minute rest period. The results showed that the position of the prostate changed during the MRI examination protocol and the volume of the bladder and rectum varied.

The use of several types of MR images for different purposes in an MRI-only workflow may be disadvantageous, due to the risk of motion between image acquisition and the introduction of systematic uncertainties. MRI sequences should thus be acquired in close succession to minimize the impact of motion between sequences. In the study described in **Paper II**, the gold fiducial marker identification, target and OAR delineation, and treatment planning tasks, were all performed in the LFOV images. This was enabled by using support images that guided the respective task in the LFOV images. The support sequences were acquired immediately before or after the LFOV sequence in the MRI examination protocol. This limited the risk of motion between image acquisitions in the MRI examination protocol, and excluded all types of image registration, in the treatment preparation phase of the workflow. However, the effects of motion are not eliminated during the MRI examination protocol by this strategy, and requires attention throughout the workflow. Tyagi et al. (2017) suggested registration between different MR images as an alternative method of dealing with motion between sequences in the MRI examination protocol, (Tyagi et al., 2017a). This required the frame of reference of the MRI examination protocol to be separated, and the images were registered with dedicated software. Using this strategy, they were able to use different MR images for target and OAR delineation, and treatment planning.

4.2 Target and OAR delineation

When all necessary pre-planning imaging has been performed, the next task is to define the volume to be irradiated. If target delineation is performed on an image not primarily used for treatment planning, systematic uncertainties may be introduced due to patient-related motion between acquired sequences. It is therefore of great importance to delineate the target and OAR in the same geometry as that in which the treatment plan will be drawn up. This can be done by delineation directly on the MR images used for sCT generation, as described in **Paper II**, or by registration of the different MR images into a common frame of reference (Tyagi et al., 2017a).

4.2.1 Volume definition and margins

According to ICRU report 50 (ICRU, 1993), the gross tumour volume is the volume in which the density of malignant cells is highest. This includes the primary tumour, with or without metastatic lymph nodes, and distant metastases. The clinical target volume (CTV), is the gross tumour volume including structures with clinically suspected involvement that have not been proven. The PTV, is an expansion of the CTV and is a purely geometric concept. The PTV margin is added to the CTV to include potential uncertainties arising from random and systematic errors in the radiotherapy workflow. This can be mathematically expressed in several ways, but the van Herk formula (van Herk et al., 2000) is commonly used (Equation 1).

$$M = 2\Sigma + 0.7\sigma \quad (1)$$

The required margin (M) is a combination of the total standard deviation of systematic (Σ) and random errors (σ). This equation is valid under the assumption that a minimum dose of 95% to the CTV will be valid for 90% of a population, and should be considered a lower limit for safe radiotherapy.

Common PTV margins for prostate cancer patients are between 3 and 10 mm, depending on the level of sophistication of the method used for alignment of the patient, patient positioning and monitoring during treatment (Yartsev and Bauman, 2016). Daily re-planning and live soft tissue monitoring during treatment delivery enable the use of small margins. Small margins, ~3 mm, have been used to treat prostate cancer patients with the MR-linac (Bruynzeel et al., 2019). The OAR of prostate cancer patients include the urinary bladder, the rectum, anal canal, penile bulb and femoral heads (Widmark et al., 2019). According to ICRU report 50, OAR are normal tissues that significantly influence the way in which the treatment plan is designed and/or the

prescribed dose. Radiation to the OAR is associated with radiotherapy-induced toxicity, such as defecation urgency, diarrhoea, faecal incontinence, proctitis and rectal bleeding (Olsson et al., 2018). Since most OAR are located close to or partially included in the PTV, such as the rectum, the dose to the OAR should be kept as low as reasonably practicable during treatment planning.

Any source of uncertainty should be removed or reduced to ensure high-precision radiotherapy. As can be seen from the van Herk formula, systematic uncertainties have a greater impact on the required PTV margin than random uncertainties. Random uncertainties, such as day-to-day variations in patient set-up, blur the dose distribution in all patients, and might result in under-dosage of the CTV. A purely systematic uncertainty, such as the delineation uncertainty, affects all treatment fractions throughout the course of treatment in an identical way for some patients (van Herk, 2004). This leads to an unknown shift of the dose distribution, relative to the CTV. While large random variations cause moderate under-dosage for most of the patient population, large systematic variations cause significant under-dosage in some patients (van Herk et al., 2000). Both variations are thus undesirable, but systematic variations may have a greater impact on individual patients. The van Herk formula assumes that several fractions are used, and that the mean random error is zero. If only a few fractions are used, as in hypo-fractionated radiotherapy, the van Herk formula must be adjusted.

4.2.2 The use of MR images for target delineation

The use of MR images reduces inter-observer variability in the delineation of the prostate (Milosevic et al., 1998, Parker et al., 2003). The use of MR images has also resulted in better definition of the prostate apex, than when using CT images (Debois et al., 1999). Several studies have shown that the delineated prostate volume was smaller when using MR images than when using CT images (Hentschel et al., 2011, Rasch et al., 1999, Seppala et al., 2015, Smith et al., 2007, Tzikas et al., 2011). In these studies, the ratio between the CT- and MR-delineated volumes ranged from 1.16 to 1.5. A smaller delineated prostate volume leads to a smaller irradiated volume, and hence a potentially reduced dose to the surrounding OAR (Figure 4).

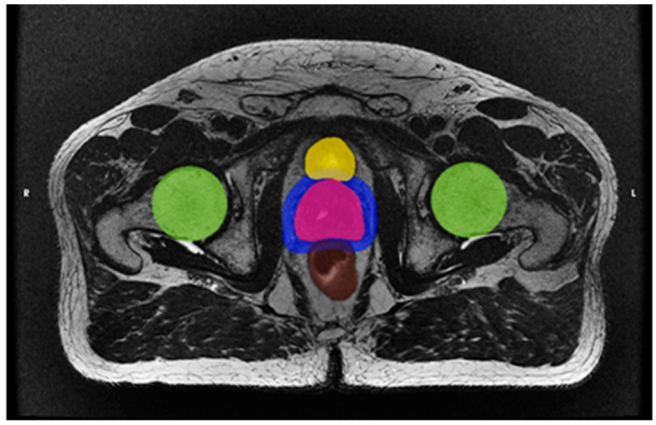

Figure 4. Delineated target structures, CTV (red) and PTV (blue), on a LFOV image, visualized in an image slice through the centre of the prostate volume. The OAR visualized include the bladder (yellow), rectum (brown) and femoral heads (green).

Training and the application of guidelines have been identified as important tools to reduce inter-observer variability in the delineation process (Segedin and Petric, 2016). In the ESTRO ACROP consensus guidelines on CT- and MRI-based target volume delineation for primary radiation therapy of localized prostate cancer (Salembier et al., 2018), T2-weighted MRI was stated as currently being the best modality for prostate delineation. These guidelines cover target and OAR delineation for the CT-only workflow and the dual-modality workflow with MR and CT images. Gold fiducial marker registration of the CT and MR images is suggested when using a dual-modality workflow, followed by extrapolation of the MR-delineated prostate volume to the CT images. Using this method, the delineated prostate volume in the dual-modality workflow should be the same as in the MRI-only workflow, since the target is extrapolated to the MR images if no other adjustment is applied.

The hypothesis that the delineated prostate volume is the same in dual-modality as in an MRI-only workflow was tested in the study presented in **Paper III**. The alternative hypothesis was that the oncologist would adjust the prostate volume to the CT geometry, resulting in a larger dual-modality prostate volume, than in the MRI-only workflow. In this study, the prostate was delineated by the same oncologist in the dual-modality workflow and the corresponding MRI-only workflow. The ratio between the CT- and MR-delineated prostate volumes was found to be 1.22, which is within the range of 1.16 to 1.5 reported in previous studies However, in these previous studies delineation was performed on MR or CT images separately, and not in comparison to the dual-modality workflow, as in our study. Our results showed that in the dual-modality workflow the clinicians delineated with respect to the CT images, as well as

the MR images. This adjustment can be explained by imperfect registration between the CT and MR images and variations in the volume of the rectum and bladder, which were accounted for in the delineation. This shows that the alternative hypothesis was valid, and that the assumption that the dual-modality and MRI-only delineated prostate volume were the same was not valid. Based on the findings of the present study, it is therefore recommended that each clinic carefully reviews their target delineation process using MR images prior to a transition from dual-modality to an MRI-only workflow.

4.3 Treatment planning

When the target and OAR have been defined in the MR geometry, the next task in the MRI-only workflow is treatment planning. A crucial task in the MRI-only workflow is the generation of sCT images (Figure 5). These images are used primarily for two purposes: 1) to enable conversion to ED used for absorbed-dose calculations during treatment planning, and 2) to create reference images for patient set-up verification prior to treatment. Important considerations in the choice of sCT image generation method are the time required for acquisition of the sCT MRI sequence, the amount of manual work, the accuracy required compared to CT-based dose calculations, and the clinical availability of the method. In the optimal implementation of an MRI-only workflow, the sCT-generation method should be included seamlessly in the existing workflow, without increasing the amount of manual work or time.

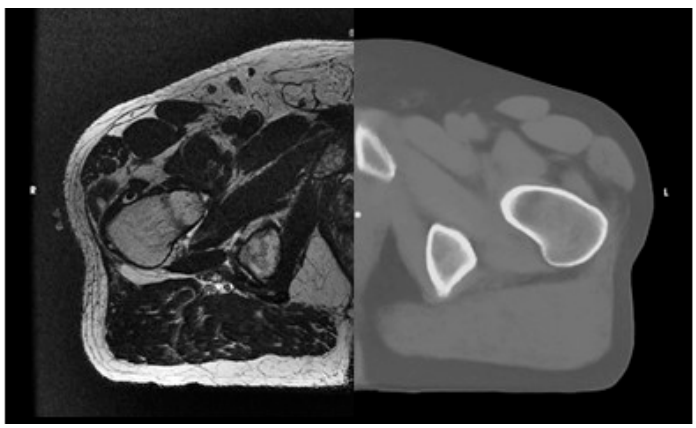

Figure 5. A LFOV T2-weighted MR image (left) and the sCT (right) generated from it using MriPlanner (Spectronic medical AB, Helsingborg, Sweden).

4.3.1 Basic principles of a synthetic CT

The concept of using MR images for treatment planning in radiotherapy has been investigated since the 1990s. The first studies presenting the feasibility of MRI-only treatment planning used bulk density strategies, where a water-equivalent HU value was assigned to the entire patient volume. Assigning a homogeneous value of attenuation inside the head in MR images in the cranial region resulted in dose differences of less than 2% compared to dose calculations based on CT images (Schad et al., 1994). A similar method of water-equivalent assignment for conformal radiotherapy has also been presented for prostate cancer patients (Lee et al., 2003). In this study, two bulk density strategies were investigated: assigning a water-equivalent value of 0 HU to the complete CT images, or a combination of assigning an average bone density of 320 HU to manually delineated bones and water equivalent to the rest of the body. Lee et al. (2003) also applied water and bone density assignments to MR images for five patients, and successfully demonstrated the feasibility of MRI-based treatment planning.

One drawback of bulk density water assignment to the entire patient volume is the lack of references for patient set-up verification, as there is no information on the bone anatomy. Manual delineation of the bones would enable set-up references (Lee et al., 2003), as was later demonstrated by Chen et al. (Chen et al., 2004). Diagnostic reconstructed radiographs (DRR) were generated based on MR images by assigning a bulk density value of 2.0 g/cm^3 to manually delineated bony structures in the pelvic area. Although this provided references images for patient set-up, manual delineation is time consuming, and not favourable in the clinical setting.

Since these initial steps towards MRI-based dose calculations, there has been a rapid increase in the number of sCT-generation methods published (Edmund and Nyholm, 2017, Johnstone et al., 2018). Methods have been developed from basic bulk-density assignments to more modern generation methods, in which multiple or continuous density values are assigned to the MR images. These modern generation methods provide images which are today commonly called pseudo-CT images, substitute CT images or, as in this thesis, synthetic CT images.

4.3.2 Generation methods

Modern sCT-generation methods can be classified into two main categories: voxel- and atlas-based methods, each with subgroups where different methodologies are applied. Various sCT-generation methods are presented in the reviews by Edmund et al. (2017) and Johnstone et al. (2018), using categorization into atlas, voxel and hybrid methods

(consisting of a combination of atlas- and voxel-based methods). Johnstone et al. (2018) define bulk density techniques as a method category (as described in section 4.3.1). The atlas- and voxel-based methods are presented below.

Atlas-based methods

Atlas-based methods make use of registered CT and MR images from patients forming an atlas. The atlas works as a dictionary, providing the best CT representation for new MR images. Atlas-based methods rely on the registration of the existing MR images in the atlas to new MR images. This is required to determine the relation between MR intensities and the corresponding CT values. The concept of an average atlas technique has been proposed for prostate radiotherapy (Greer et al., 2011). In their workflow, an average atlas was created from a population of prostate cancer patients by registration of the corresponding MR images. The MR images in the average atlas were deformably registered to the new MR images, and the prostate and OAR were automatically defined. After manual adjustment of the delineated structures, when necessary, EDs were mapped to the MR images using the known deformation, and a corresponding average CT atlas. This method belongs to the *single-atlas* category where either one patient, or an average patient created from multiple MR and CT image pairs, is used.

Multi-atlas methods have also been presented, using multiple MR and CT image pairs. The MR images for each patient in the atlas are registered to the new MR images. A voxel patch comparison, normalization and similarity weighting were then used to estimate the HU of the new MR images (Dowling et al., 2015). This method falls under the sub-category of pattern recognition and patch-based methods. Since voxel information was used to create the final sCT images, this sub-category of generation methods is partially voxel-based. Nevertheless, generation relies on a registered atlas, in contrast to purely voxel-based methods, where accurate image registration is not necessary (Dowling et al., 2015, Jonsson et al., 2013).

Atlas-based methods often require a single standard MRI sequence, thus imaging is relatively short and uncomplicated. However, atlas methods can be developed using images from multiple MRI sequences. The use of an atlas also enables automatic delineation of structures, which can further optimize the workflow and reduce inter-observer delineation variability (Johnstone et al., 2018). Problems associated with atlas methods are related to aberrant patient anatomies that deviate from the atlas, either in terms of weight or due to anatomical abnormalities (Dowling et al., 2015). Since these methods also rely on image registration, they can be considered contradictory, since the reduction in systematic image registration uncertainties is one of the main reasons for using MRI-only workflows.

Voxel-based methods

Voxel-based methods rely on the intensities in MR images from one or several MRI sequences. Standard MRI sequences or ultrashort echo-time (UTE) sequences can be used. UTE sequences allow better imaging of bones, as they have a short T2* relaxation time, but has only been used in brain (Edmund and Nyholm, 2017, Johnstone et al., 2018). The use of standard MRI sequences has been demonstrated in prostate cancer patients (Kapanen and Tenhunen, 2013). Using a T1/T2*-weighted GRE sequence allowed a model of the relation between MR intensity and HU values to be created based on 40 randomly chosen bone voxels in MR and CT images from ten patients. After manually delineating the bones in the MR images, the bony structures were divided into 16 subgroups and their mean MR intensities were converted into HU using the model. The remainder of the body was assumed to be water equivalent. This model was later developed to include the relationship between MR intensity and HU for tissues other than bone, such as muscle and fat, and urine (Korhonen et al., 2014).

Accurate image registration of the new MR images is not required in voxel-based methods (Dowling et al., 2015, Jonsson et al., 2013). Atypical anatomy is better accounted for than in atlas-based methods. The use of UTE images has made automatic classification of cortical bone possible. However, these sequences are considered specialized, and not typically part of the clinical MRI examination protocol. One concern when using standard MRI sequences is the difficulty in differentiating between bone and air, requiring manual delineation of bony structures in many cases. Manual delineation can be time consuming and is therefore undesirable in the clinical setting. One drawback of using multiple sequences in voxel-based approaches is the longer scanning time, which increases the risk of motion between sequences (Johnstone et al., 2018).

Deep learning

Deep learning is a subfield within machine learning in artificial intelligence. Deep-learning approaches in general consist of multiple-layer networks; convolutional neural networks and generative adversarial networks, being two examples that have been used in radiotherapy applications (Sahiner et al., 2019). Mathematical models are created using these types of network and the network learns to capture and represent relationships between the input and output. Deep learning approaches for sCT generation have emerged in recent years. In these approaches, the network is trained to learn the relationship between CT and MR images. The input to the network is an MR image, and the output the corresponding CT image created by the network (i.e. an sCT image). The first demonstration of a deep learning convolutional neural network for sCT image generation was presented in 2017 (Han, 2017). Synthetic CT images were

created in seconds using rigidly registered CT and MR images of the brain from 18 patients. Although the method was restricted to a single slice, the training material was limited, and no dosimetric evaluation was made, it demonstrated the feasibility of fast sCT image generation using a convolutional neural network. Following this, methods for deep-learning sCT image generation for the male pelvis have been presented and dosimetrically evaluated for radiotherapy of patients with prostate cancer (Chen et al., 2018, Maspero et al., 2018).

After successfully training a network, sCT image generation is very fast, and training does not have to be repeated. However, networks that rely on image registration in the training data are sensitive to misalignments between the CT and MR images. Misalignment in the training data will lead to inaccuracy in the method, as it has been trained to make a false prediction (Han, 2017). Deep learning are restricted to the way in which training of the network is performed and the quality of the training data. A network can only produce sCT images if the input MR images resemble the training material used in the network. One attractive application of sCT deep-learning approaches is the MR-linac, where the sCT images are required instantly after MR imaging (Arabi et al., 2018).

Commercial solutions

The decision regarding which sCT image generation method should be used in the implementation of an MRI-only workflow is important. Hospitals require that products used in the clinical workflow must be developed by the hospital itself, are used within a research project, or are clinically approved. Commercialization of a product can make the process of implementation more straight forward, since this means that the product are distributed and managed by a company. Approval of medical equipment is given by Conformité Europeéne approval (CE marking), or the US Food and Drug Administration (FDA approval). Commercialization and regulatory approval increases the potential of a wide spread adoption of MRI-only.

The majority of published sCT-generation methods have been developed in-house. This means that the software and/or underlying source code belongs to a research group within, or associated with, a hospital, and the methods have been developed and tested within approved research studies. It is difficult for hospitals to implement methods developed at other hospitals, and commercial solutions are more commonly used. Four out of the six implementation studies in Table 1 (Christiansen et al., 2017, Tyagi et al., 2017a, Kerkmeijer et al., 2018, Persson et al., 2018a) employed one of the two commercially available sCT-generation methods, MRCAT™ (Philips, Helsinki, Finland) or MriPlanner™ (Spectronic Medical AB, Helsingborg, Sweden).

Philips was the first company to introduce a commercial sCT solution called MRCAT (Köhler et al., 2015). The initial version of this generation method performed tissue classification based on a DIXON sequence. The new MR images were divided into five tissue types: air, water, fat, cortical bone and spongy bone, using automatic, model-based segmentation. This method belongs to the voxel-based methods, but also adopts a bulk density approach. The workflow and dosimetric evaluation of MRCAT were presented by several groups in 2017 (Tyagi et al., 2017b, Christiansen et al., 2017, Kemppainen et al., 2017). This was later followed by the commercialization of MriPlanner, which was the sCT-generation method used in the studies described in **Papers II**, **IV** and **V**. This multi-atlas-based sCT-generation method with a statistical decomposition algorithm, was first described by Siversson et al. (Siversson et al., 2015). In this method, deformable image registration is followed by multiple segmentations. Candidate sCT images are created by applying deformation to candidate CT images in the atlas. The candidate sCT images are then fused together voxel-wise by calculation of the weighted median HU, and a final sCT image is created.

Both MRCAT and MriPlanner are dependent on segmentation, as well as several image registrations. Since MRCAT is supplied by an MR-scanner vendor, sequence for sCT generation, as well as the sCT generation itself, are available directly in the MR scanner. This method is thus preferable and easily adopted by hospitals with Philips MR scanners. In contrast to MRCAT, MriPlanner is MR-vendor independent, meaning that it can be used with MR scanners from different vendors (**Paper IV**). The conditions for the widespread implementation of MRI-only workflows with this technique are thus better, although the software is not supplied ready to use with the MR scanner, as in the case of MRCAT for Philips users.

4.3.3 Treatment planning using a synthetic CT image

Since treatment planning is traditionally based on the use of CT images acquired with a CT scanner, the treatment planning system (TPS) does not completely comply with the use of MR images (Schmidt and Payne, 2015). In MRI-only workflows, the sCT images generated are imported into the TPS, and should ultimately be used in the same manner as normal CT images. In an MRI-only-compatible TPS, the sCT images would be used in the background, for QA purposes, and the MR images should be the primary images used for treatment planning. However, this is not possible in most TPSs today, and sCT images are therefore used as the primary images. This means that the sCT images are visible throughout the treatment planning procedure, and the MR images are not used after delineation. The target and OAR are transferred to, or created directly on, the sCT images (Figure 6).

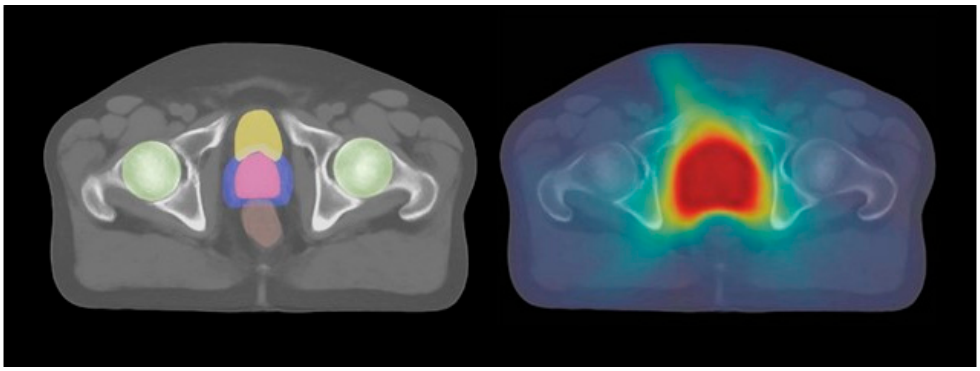

Figure 6. Target, including the CTV (red) and PTV (blue), and OAR including the bladder (yellow), rectum (brown) and femoral heads (green), created directly on sCT images. A treatment plan is created according to the prescribed dose and clinical DVH criteria, resulting in a calculated dose matrix. The image on the right shows a dose matrix overlaid on an sCT image through the central slice of the prostate, with a dose ranging from 0 Gy (light blue) to 78 Gy (dark red).

There are some general differences in the use of sCT images and CT images in a TPS. In the studies described in **Papers II**, **IV** and **V**, the TPS Eclipse from Varian Medical Systems was used. Factors that are affected when Eclipse is used are the position of the couch structure, user origin definition, ED conversion and the creation of reference images for patient set-up. The general differences, compared to CT-based treatment planning, are presented below. Other factors may come into play when other TPSs are used, but only the Eclipse TPS is considered in this thesis.

Couch position

The insertion of a virtual couch in the TPS enables correction for the attenuation of radiation by the treatment couch, making the dose calculations more accurate. The virtual couch is usually placed at a distance corresponding to the thickness of the support used for patient immobilization during CT imaging. The threshold can be adjusted in CT images to enable visualization of the patient immobilization device and the CT couch. The virtual couch can then be inserted at the correct distance from the body. The MR couch is poorly visible or not visible at all in MR images, depending on the sequence used. The couch is not represented in the generation of sCT images, and the distance between the patient's body contour and the MR couch must be known. An MRI sequence can be added for couch visualization to obtain the correct distance, but this prolongs the MRI examination protocol, and is therefore undesirable. The most convenient way to account for attenuation in the couch is to use the same immobilization device for all patients, thus standardizing the distance between the patient and the couch. Prostate cancer patients normally lie on a thin mattress during MRI

examination and treatment, and its thickness can be used as the distance at which the virtual couch should be placed beneath the patient.

Definition of the user origin

In the TPS, the intersection of the marks made on the patient's skin during patient immobilization is defined as the image origin, commonly called the user origin. Knowing the distance between the user origin and the treatment plan isocentre helps when positioning the patient correctly for pre-treatment imaging. The marks on the skin can be visually represented in CT images by placing highly attenuating material over them. In MR images, liquid markers such as "PinPoint for image registration 128" (Beekley Medical, Bristol, Connecticut, USA), can be used (Figure 7). Tattooless radiotherapy workflows have also been presented, where no skin marks are used.

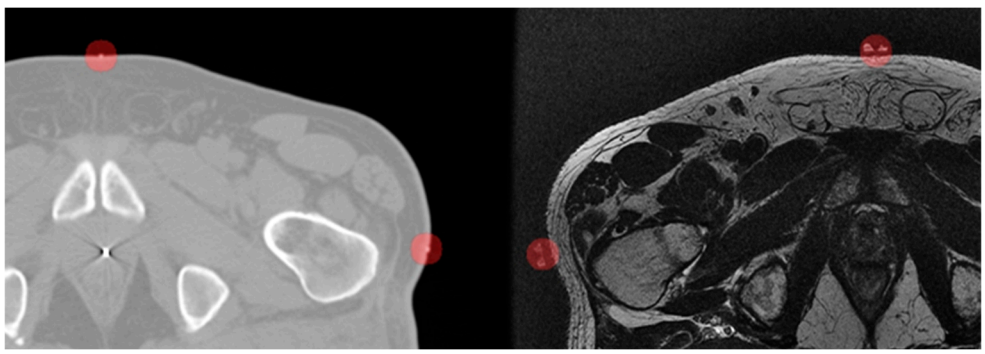

Figure 7. The definition of the user origin in CT images is based on the use of high-density objects placed on the surface of the patient (red circles, left image). In MRI, liquid markers can be used for user origin definition. In the MR image on the right the "PinPoint for image registration 128" marker has been used which has a doughnut shape, forming a distinctive valley in the middle (red circles, right image).

ED conversion

To enable dose calculation, the HU in the sCT images must be converted to ED. This is done using conversion curves, based on HU with corresponding ED values, for different materials (Knöös et al., 1986). Conversion curves can be based on theoretical values published in the literature, or on measurements performed at the CT scanners used for treatment planning at the hospital. The conversion curve is inserted in the TPS, allowing the absorbed dose to be calculated. Different strategies can be used for HU to ED conversion in MRI-only workflows. Either the same calibration curve as for CT-based treatment planning can be used (Christiansen et al., 2017, Tyagi et al., 2017a), or a calibration curve from the vendor of the sCT-generation method can be applied (Kemppainen et al., 2017). HU to ED conversion has been reported as a

confounding factor in MRI-only workflows (Maspero et al., 2017a). A relative dose difference of 0.7%±0.2% was seen as a result of using the clinical conversion curve, rather than the vendor supplied curve for MRCAT. It is thus important to validate the HU to ED curve intended for treatment planning in the MRI-only workflow. The clinical HU to ED conversion curve was used in the studies described in **Papers II**, **IV** and **V**.

Reference images for patient set-up verification

Treatment planning includes generating reference images for patient set-up verification prior to treatment delivery. Depending on the set-up verification strategy chosen, the sCT images or 2D-based DRR from the sCT images can be used (Kemppainen et al., 2018, Korhonen et al., 2015, Tyagi et al., 2017b). MR images have also been used directly and displayed at the treatment unit (Wyatt et al., 2019). When the sCT images are used directly, either the bony structures or the identified fiducial markers are used. When DRR are used, a pair of images is generated from the sCT images in the TPS. For prostate cancer patients, where fiducial markers are commonly used for patient set-up, the fiducials must be represented in the DRR. This can be done in two ways: by delineating the fiducials and representing them as structures in the DRR, or by representing the marker coordinates as physical objects in the images (Figure 8).

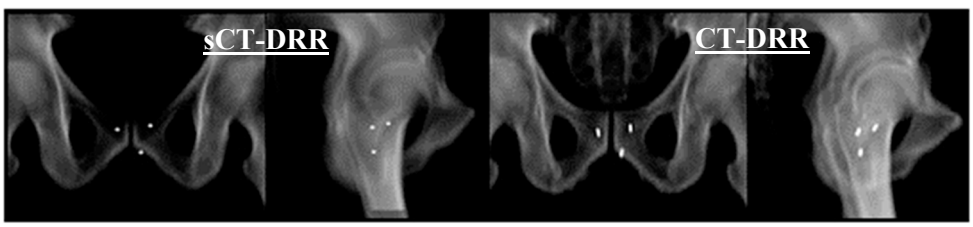

Figure 8. DRR created from sCT images and CT images. Fiducial markers were inserted into the patient, seen as spherical objects in the sCT-DRR (left), which have been burnt into the sCT image. In the CT-DRR (right) the fiducial markers are seen as cylindrical objects representing the artefacts from the fiducial markers in the CT image.

4.3.4 Validation of synthetic CT images for treatment planning

The validation of sCT images for treatment planning has traditionally been performed using the CT images as the ground truth. Comparisons of dose distributions, HU values and bone segments are commonly used (Edmund and Nyholm, 2017). Since the primary objective of sCT images is to create a foundation for treatment planning and calculate the dose, the main interest lies in the dosimetric accuracy of the sCT images. The dosimetric accuracy in this case refers to the difference between dose distributions resulting from calculations using CT images and sCT images. The dose distribution obtained from CT images is considered the true value in the comparison. There is considerable variation in the methods used for comparison in published papers on sCT-generation methods, and there is no consensus on how sCT-generation methods should be validated.

The MR-Only Prostate External RAdiotherapy (MR-OPERA) study (**Paper IV**) validated the multi-atlas method presented by Siversson et al. (Siversson et al., 2015). This study was the first multi-centre study to validate an sCT-generation method for treatment planning. Four hospitals, two MR vendors (Siemens and GE), field strengths of 1.5 T and 3 T, and a total of 170 prostate cancer patients were included in the study. Validation was performed as follows.

1. The target and OAR were delineated on the CT images.
2. A CT treatment plan was created and the dose distribution calculated.
3. sCT images were registered and resampled to the CT geometry.
4. The sCT images were imported into the TPS.
5. The CT treatment plan was transferred to the sCT images.
6. The sCT dose distribution was calculated with fixed plan parameters.
7. The resulting CT and sCT dose distributions were compared.

Each hospital followed steps 1-7, and their clinically created CT treatment plans were recalculated on generated sCT images for their own patients. The calculated CT and sCT dose distributions were compared using DVH comparison for targets and OAR and gamma analysis. The mean dose differences between the CT and sCT dose distributions were less than 0.3% of the prescribed dose for all investigated dose criteria. The median dose differences at the four hospitals were similar, with maximum differences of less than 1.5% of the prescribed dose for target and OAR mean doses. The mean gamma pass rate was greater than 97% for a global gamma criterion of 1%/1mm, using a 15% dose cut-off. Similar results were obtained in the implementation study described in **Paper II**, where the maximum dose differences were less than 2% of the prescribed dose, after correction for rectal gas. Gamma pass rates were above 98% for a global gamma criterion of 2%/1mm using a 15% dose cut-off. This is in line with

previously published results on synthetic CT generation methods for prostate, where the dosimetric accuracy ranged from 0.0 to 2.0% for voxel- and atlas-based methods (Edmund and Nyholm, 2017, Johnstone et al., 2018). Bulk density approaches in general show higher deviations, of up to 9.7% in the target volume, depending on the HU assignments. Assigning a combination of water and bone HU values instead of solely water equivalent HU has consistently shown better dosimetric accuracy. The commercial software MRCAT showed good dosimetric accuracy for prostate cancer patients, with maximum differences of about 2%, and gamma pass rates above 93% (1%/1mm) and 99% (2%/1mm) (Christiansen et al., 2017, Kemppainen et al., 2017, Tyagi et al., 2017b). Deep-learning-based approaches have also shown good dosimetric accuracy between CT and sCT dose distributions. Reported maximum deviations in DVH parameters are below 2.5% (Maspero et al., 2018), and gamma pass rate above 98% for a gamma criterion of 1%/1mm (Chen et al., 2018).

Considerations and potential pitfalls

The treatment plan created for the validation of sCT images for treatment planning should reflect the treatment technique and prescription to be used in clinical routine. A conventional three-field treatment technique will be affected by the anatomy in the radiation pathway, while a volumetric modulated radiation therapy plan, in which the radiation is spread over 360 degrees, may be affected differently. The use of different types of radiation in the workflow, such as photons or protons, may also affect the dose comparison between CT and sCT dose distributions differently. The feasibility of a prostate MRI-only workflow for proton treatment planning, currently in use for photon treatment planning, was recently evaluated, showing promising results (Aramburu Nunez et al., 2020).

Registration is needed to transfer the treatment plan from the CT to the sCT images. This image registration can be either deformable or rigid, and can be performed directly in the TPS or using external software. Deformable image registration acts on each voxel of the image volume, depending on the algorithm used, and deforms one image to fit a reference. Deformable image registration can create very exact registration between images, but can also introduce non-realistic deformation of the images. For example, if deformation of the bones is allowed, a generation error in a bone segment of the sCT images can be masked by the deformable registration. Rigid image registration can be performed using three or six parameters, i.e. translational directions only, or both translation and rotation. Rigid registration acts on the complete image volume and moves the image around a fixed point, instead of deforming individual voxels. Differences in body contours are maintained in rigid image registration, which can affect the dose comparison.

If image registration is performed in the TPS, extra attention must be paid to the transfer of the treatment plan using the image registration. Plan transfers in TPS are often performed in translational directions only. As a result, the treatment plan will only be transferred using the translational directions of the image registration, neglecting any rotation in the registration matrix. This will result in a slightly rotated treatment plan compared to the image volume, if a six-parameter rigid image registration has been used. This mainly affects dose comparisons in areas away from the registration centre.

In dose comparisons between the CT and sCT dose distributions, it is important to consider the impact of slice thickness and voxel size in the CT and sCT images. One strategy for DVH comparison is to transfer the target and OAR volumes from the CT images to the sCT images. If the two images have different voxel sizes, the transferred volumes will change slightly to fit the new image geometry. This will affect the DVH comparison in a manner depending on the magnitude of the volume change. An alternative solution is resampling into a common voxel size, prior to transferring the target and OAR and dose recalculation. The dose matrices can also be resampled with external software, enabling DVH comparison with the same volumes.

The impact of patient repositioning between CT and MR imaging sessions is a problem often discussed in connection with the validation of sCT-generation methods. To minimize this bias, deformable image registration can be used prior to re-calculation of the treatment plan (Kemppainen et al., 2017). A simpler strategy is to assign an outer body contour corresponding to the CT images to the sCT images. This can be done by replacing any areas containing air inside the CT body contour with water, and removing tissue outside the CT body contour. This correction strategy was successfully demonstrated in **Paper IV**, where the median and maximum differences for the corrected sub-population were reduced (Figure 9).

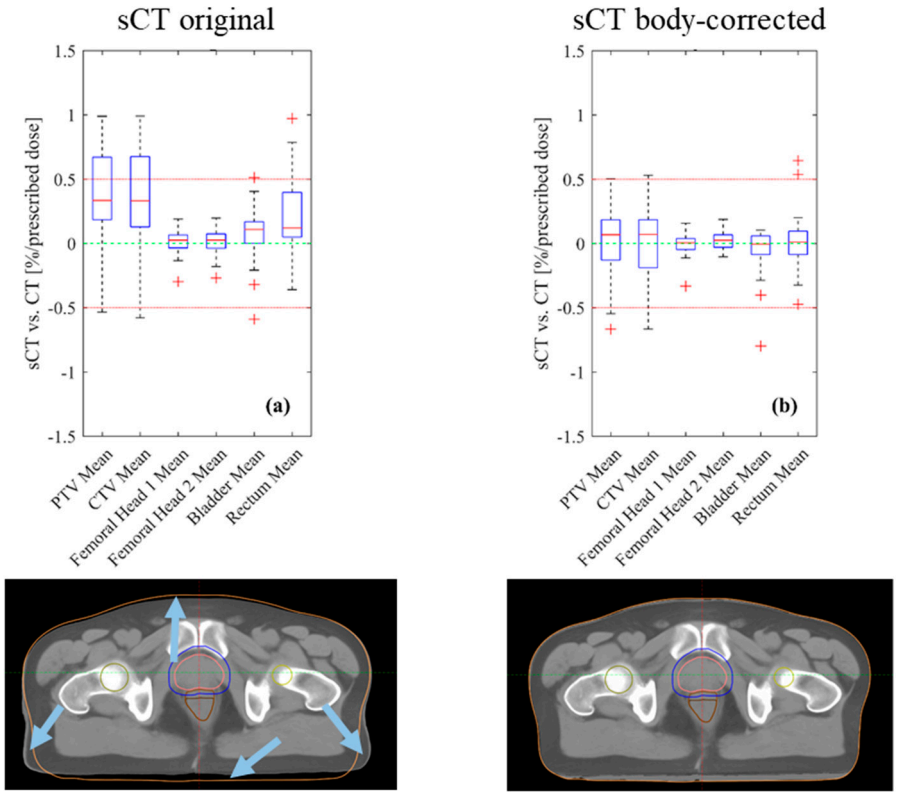

Figure 9. Demonstration of the body contour correction used in the study presented in **Paper IV**. The outer body contour of the CT images was overlaid on the original sCT images (bottom left). Any air inside the CT contour or soft tissue outside the CT contour (indicated by the blue arrows) was replaced with water or removed, resulting in a body-corrected sCT image (bottom right). The dose comparison for a population of 28 patients is shown in the box plots. The original sCT-CT dose comparison is shown on the left and the body-corrected sCT-CT dose comparison on the right. (The figure is adapted from Fig. 3 in **Paper IV**).

The internal anatomy of the patient may also change between the CT and MR imaging sessions. This was seen in three patients in the study described in **Paper II**. The initial dose comparison between CT and sCT dose distributions for these patients showed differences exceeding 4% of the prescribed dose, to either the target area or the rectum. After further investigation, this was found to be caused by rectal gas in close proximity to the CTV in all three patients. In the sCT-generation method used in this study, air is represented by soft tissue in MR images. This is motivated by the fact that air cavities are unlikely to appear in the same place during each fraction of the treatment. When creating or recalculating the treatment plan using CT images, large air cavities should be noted and the impact on the dose comparison investigated.

4.4 Patient set-up verification

Prior to treatment delivery, the patient set-up must be verified, based on registration between the reference images and the pre-treatment images acquired with the treatment unit. This ensures alignment of the patient to the plan isocenter, and is usually called image-guided radiotherapy.

Prior to pre-treatment imaging, the patient is aligned using the skin marks created during MR imaging. Surface guidance is an alternative to skin marks. Using surface guidance, more information on patient posture was obtained for breast cancer patients, where optical light was projected onto the surface of the patient (Kugele et al., 2019). Skin marks have not previously been considered a reliable representation of the position of internal structures in the pelvic area (Verhey, 1995). Recommendations on image guidance for prostate cancer treatment are given in the ESTRO ACROP consensus guidelines on the use of image-guided radiation therapy for localized prostate cancer (Ghadjar et al., 2019). These guidelines state that patient set-up with laser and surface systems could be used as a complement, but cannot completely replace image-guided radiation therapy. Furthermore, they recommend that image guidance should be performed based on the prostate itself, preferably using fiducial markers and CT-based imaging. Cone beam CT (CBCT) imaging is an example of CT-based pre-treatment imaging. Electronic portal imaging devices and kV images are alternatives to this, however, their use in the detection of prostate deformation and rotation may be limited. Daily imaging is recommended in the guidelines, due to the benefits regarding rectal toxicity and biochemical progression-free survival, compared to weekly imaging protocols (de Crevoisier et al., 2018). A daily correction strategy is more efficient in reducing both random and some systematic errors, compared to a weekly schedule. It has also been suggested that the PTV margin should be adapted based on the set-up strategy used, and kept to a minimum by daily correction strategies and tracking (Ghadjar et al., 2019).

4.4.1 Set-up verification in an MRI-only workflow

Patient set-up verification in an MRI-only workflow does not differ in principle from that in the dual-modality workflow. The aim is to position the patient correctly relative to the treatment plan isocentre and reduce systematic and random errors. Using the set-up strategy of choice, the sCT or MR images are used, instead of the conventional CT images. The patient set-up can be verified using fiducial markers, bony anatomy or soft tissue.

Two approaches have been demonstrated using bony anatomy for patient set-up in MRI-only workflows. In the first, the sCT-DRR generated were registered to kV images (Kemppainen et al., 2018), while in the second, sCT images were registered to CBCT images (Korhonen et al., 2015). Soft tissue CBCT image registration has also been presented, where the MR images were imported into the treatment unit by changing the image modality DICOM tag in the MR images to "CT". This enabled visualization of the MR images at the treatment unit, and the CBCT images could then be registered to the MR images (Wyatt et al., 2019). Automatic registration of MR and CBCT images has been hampered by insufficient bony tissue representation in the MR images, which caused system warnings (Korhonen et al., 2015). Non-compliance of the patient in bowel preparation prior to MR and CT imaging has been reported to cause systematic differences, which affected the initial registration between CT and MR images in the anterior-posterior direction in one patient. After exclusion of this patient, similar margins were found for CT-CBCT and MR-CBCT set-up strategies (Doemer et al., 2015).

If fiducial markers are used for patient set-up verification, they must be represented in the sCT images. This can be achieved by using the positioning of markers identified in the MR images, and representing them as a physical object or a structure (**Paper II**). Tyagi et al. (2017b) investigated fiducial marker registration to kV and CBCT images. The fiducial markers were segmented in the fiducial marker identification sequence and the regions of interest were transferred to the sCT images. The markers were also burnt into the sCT images by assigning the voxels in the regions of interest a HU value of 3000. A similar approach was used recently, where delineation of the identified markers was used as the reference for patient set-up with kV or CBCT images (Greer et al., 2019). Prior to the implementation of an MRI-only workflow, the chosen set-up strategy should be validated before the CT images are completely excluded from the workflow.

4.4.2 Validation of MRI-only set-up strategies

In comparison to the number of studies published on sCT generation and the geometric and dosimetric evaluation of these methods, the number of studies investigating patient set-up accuracy in MRI-only workflows is small. Only a few set-up studies were identified in the reviews by Johnstone et al. and Bird et al. (Bird et al., 2019, Johnstone et al., 2018). Validation of MRI-only set-up strategies has traditionally been performed with CT images. In this case, the set-up accuracy refers to the difference in registration to the pre-treatment images, performed with sCT (or MR) and CT images. CT image registration is considered the true value in the comparison. As in the

validation of treatment planning, validation of set-up strategies may be influenced by factors other than the quality of the sCT images. Registration methods used for set-up verification may be automatic, manual, or a combination. If performed manually, image registration may be influenced by an inter-observer bias, while automatic image registration can be influenced by the choice of registration parameters and regions included in the registration. Differences between MRI-only and CT-based set-up verification are also influenced by the image used for registration, i.e. sCT or MR images.

In general, the validation of an MRI-only based set-up strategy can be performed using the following steps.

1. Registration between sCT/MR images and CT images.
2. Registration of sCT/MR images and CT images, or corresponding DRR, to the pre-treatment images (Figure 10).
3. Comparison of calculated couch shifts between image registrations.

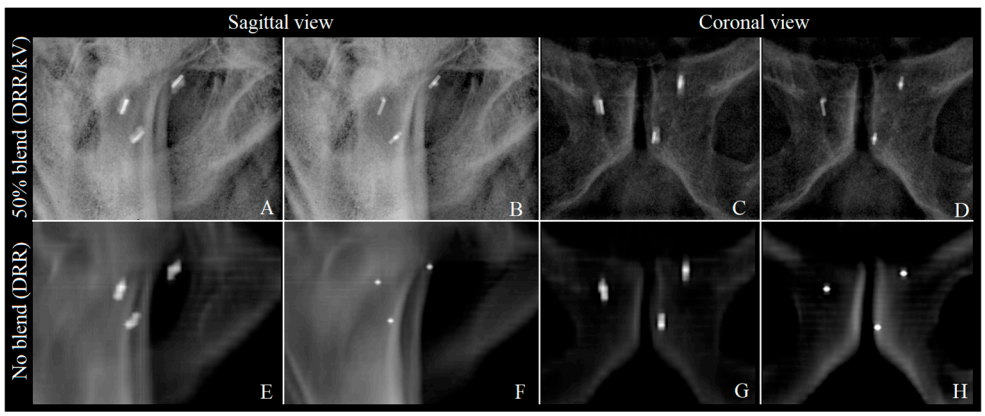

Figure 10. Fiducial marker registration using a CT-DRR (sagittal view A, coronal view C) compared to an sCT-DRR (sagittal view B, coronal view D) (A-D images with a 50% image blend between DRR and kV-images in the module used for offline review). Corresponding DRR without a kV image blend for CT-DRR (sagittal view E, coronal view G) and sCT-DRR (sagittal view F, coronal view H) are also shown.

In one of the first studies to investigate the potential of MRI-based patient set-up for prostate cancer patients, a density of 2 g/cm^3 was assigned to the delineated bones (Chen et al., 2004). The bones delineated on the MR images were within 2-4 mm of those in the CT-DRR. This study did not validate the use of the DRR in a set-up strategy by performing an actual image registration. Other studies have since been presented in which different MRI-only set-up strategies for prostate cancer have been validated. Korhonen et al. (2015) investigated patient set-up using the bony anatomy

in both CBCT images and planar images. Registration of CT-DRR and heterogeneous sCT-DRR to kV images resulted in differences of less than 2.8 mm between the two registrations. The mean differences between sCT-based and CT-based patient set-ups using CBCT images were less than 1.2 mm, but depended on the strategy and anatomy included in the CBCT image registration. In two of the nine CBCT set-up strategies evaluated, no outliers were found, whereas the remaining seven strategies had outliers that exceeded 3 standard deviations (SD). These outliers were excluded from the CBCT image registration results. MR-CBCT image registrations in general showed more outliers than sCT-CBCT image registration. Doemer et al. (2015) reported the maximum mean difference in their MR-CBCT patient set-up to be -0.15±0.25 cm in the anterior-posterior direction. This is in accordance with the results given by Korhonen et al. (2015), but without outlier exclusion. Manual alignment, as used by Doemer et al. (2015), could potentially reduce the number of outliers. Whyatt et al. (2019) found that manual MR-CBCT image registration in general differed from CT-based image registration by less than 3.3 mm. Differences in rectal filling between images was the cause of one outlier.

Kemppainen et al. (2018) and Tyagi et al. (2017b) both validated MRCAT for patient set-up verification. Kemppainen et al. found mean differences of less than 0.5 mm for a kV set-up strategy, and found both systematic and random uncertainties. They concluded that if the registration errors between CT and MR images in the dual-modality workflow were greater than 1.7, 1.5 and 1.1 mm (in the vertical, longitudinal and lateral directions), MRCAT could be considered more accurate in terms of total accuracy. Tyagi et al. found maximum differences of less than 2 mm in kV and CBCT image set-up strategies. Prostate rotation between images was found to cause significant differences. Deep-learning approaches have also been investigated in the context of patient set-up verification, showing mean translational vector distances of less than 0.6 mm for CBCT image registrations (Fu et al., 2019). In summary, patient set-up using bone and soft tissue in sCT and MR images for prostate cancer patients has been shown to be clinically feasible.

Fiducial markers are most common and one recommended set-up strategy for prostate cancer patients (Ghadjar et al., 2019). This could explain the small number of sCT-generation methods evaluated for MRI-only patient set-up. Patient set-up strategies using fiducial markers does not rely on the performance of the sCT image generation, but identifies their origins much earlier in the workflow, i.e. during MRI. The accuracy of the fiducial marker set-up strategy is determined by how well the fiducial markers can be identified in the MR images. This was briefly discussed in the section 4.1.2, and is an important task in the MRI-only workflow.

The use of fiducial markers for patient set-up verification was investigated together with an automatic CBCT image set-up strategy using bone (**Paper II**). The maximum difference between CT and sCT image registrations for the CBCT image set-up strategy was less than 2 mm for all but one patient. In this case, it was hypothesized that the larger difference was caused by difference in rotation of the patient during CT and MR imaging. Differences in the fiducial marker registrations using DRR registered manually by one observer towards kV images were less than 2 mm. The inter- and intra-observer variations in the set-up strategies were not considered in this thesis. Furthermore, only translational directions were included in the investigated image registrations. Rotational differences could also be important, and should be considered if rotational correction strategies are to be used, as when using a 6-dimensional treatment couch.

4.5 Quality assurance in clinical routine

The clinical MRI-only workflow illustrated in Figure 1 is a simplified version, intended to provide an overview. In reality, many steps are required to evaluate the performance of a radiotherapy workflow. The terms “quality assurance” and “quality control” are often used when discussing the radiotherapy workflow. QA concerns all aspects of the radiotherapy process, and includes processes to ensure consistency and safe delivery of the prescribed dose. Quality control is a specific part of this process, where the actual quality of the performance is measured and compared to a standard (IAEA, 2005). For the sake of simplicity, the term QA will be used in the rest of this section to refer to the overall process, as well as individual parts of the process.

As described in sections 4.3 and 4.4, CT images have constituted an important foundation in the validation of sCT-generation methods. Both MRI-only dose calculations and set-up strategies have been validated using comparison towards CT images. Comparison towards CT images, i.e CT-QA, has also been used in prospective implementations (**Paper II**). In **Paper II**, the CT-QA was used as a final step in the implementation of the workflow to verify fiducial marker identification as well as the sCT dose calculations. All patients in the study passed the CT-QA within acceptable levels. Electronic checklists were also used as guidance, and for error prevention, and all the checklists could be successfully completed for all patients in the study. Nevertheless, there is still room for patient-specific QA in the MRI-only workflow. It could be argued that the performance of the sCT-generation method should be verified according to an established standard, for the same reasons that QA is performed on the CT scanners used for radiotherapy. However, there is no known standard for QA of

the different tasks in the MRI-only workflow, and individual hospitals will employ their own criteria until standards are established.

When the MRI-only workflow has been implemented and is ready for routine clinical use, there will be no need for CT imaging, and the CT-QA will thus not be included. A substitute to the CT-QA will therefore be needed to enable patient-specific QA. A CT-independent QA method for error detection in sCT images used for treatment planning is presented in **Paper V**. The intention was to present a clinically feasible method of patient specific QA in MRI-only radiotherapy using CBCT-images (Figure 11). The concept was based on a previously presented method, where CBCT images were suggested for QA of sCT images of the brain (Edmund et al., 2015). In that study, a statistical approach was suggested for the validation of the sCT images. In the study described in **Paper V** a CBCT-based dose comparison was of interest, since dose comparisons have traditionally been used for the validation of sCT images. A CBCT-based dose comparison could thus be easily implemented, and the results simple to interpret. In order to replace the CT images with CBCT images, it was required that comparable dose differences were obtained when the sCT-treatment plan was re-calculated using either the CT or the CBCT images. The CBCT imaging system was found to be stable in terms of variations in HU over time, which was also considered a requirement. The re-calculated CT and CBCT dose distributions were found to be similar; the greatest difference in the PTV mean dose being 0.6%. This difference is very small, and would not have resulted in any changes in the clinical decisions. Gross errors were introduced into the sCT images for one patient, which were reflected similarly in the CT and CBCT dose re-calculations. Large errors were required in the sCT images to reach dosimetric differences greater than 2% in the PTV mean dose. An advantage of using CBCT images for QA of sCT images is that the image modality is available at the treatment unit. This facilitates the acquisition of the CBCT images at the time of the first treatment, and thus no extra imaging session is required.

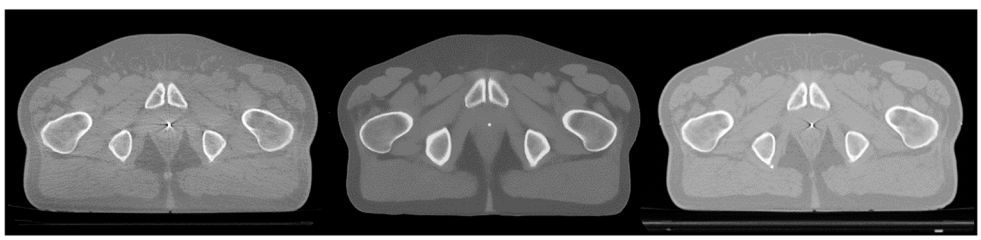

Figure 11. CBCT image of a centre slice of the prostate (left) and corresponding sCT (middle) and CT (right) images. A fiducial marker can be seen as a white, high-intensity object in the central part of each image.

The CBCT images also have the potential for use in verifying the positions of the fiducial markers identified in the MR images. An extra scheduled CBCT imaging session has been used for verification of fiducial markers in an MRI-only workflow (Tyagi et al., 2017a). This enabled verification in a separate session from the treatment, which could be advantageous as it allows QA prior to dose delivery. An alternative method for CT-independent QA of the gold fiducial marker positions is to use kV images acquired using a C-arm during marker implantation (Gustafsson et al., 2018). Bulk density dose calculations have also been suggested for QA of sCT images. These can validate the dose calculated with sCT images, and a standalone imaging modality is thus not required. However, this method cannot be used to verify the positions of gold fiducial markers.

5 Conclusions

One of the main reasons for implementing MRI-only workflows is to reduce image registration uncertainties. In the work described in this thesis, the observer bias in a common fiducial marker image registration approach was investigated (**Paper I**). Observer bias was found to be present, and in some prostate cancer patients it was of the order of 3 mm, which would have introduced a significant systematic error. It was concluded that image registration based on gold fiducial markers was associated with uncertainties. Thus, an MRI-only workflow for patients with localized prostate cancer was deemed to be beneficial, in terms of reduced image registration uncertainties.

Successful implementation of an MRI-only workflow for localized prostate cancer was demonstrated (**Paper II**). The approach using a prospective CT-QA, enabled the safe implementation of the workflow. An image-registration-free workflow was presented, where the final decisions were based on MR images from a single MRI sequence. Acceptance criteria for parts of the workflow could be determined, providing a good foundation for future clinical implementation.

Implementation of the workflow was preceded by studies to investigate target delineation (**Paper III**) and treatment planning (**Paper IV**) in an MRI-only workflow. The prostate volume in the dual-modality workflow is influenced by the difference in patient position between imaging sessions, as well as the image registration between the CT and MR images. Prostate target delineation in the MRI-only workflow led to a smaller prostate volume than in a dual-modality workflow employing CT and MR images. The hypothesis that a dual-modality prostate volume is delineated using only the MR images, and thereby equal to an MRI-only delineated prostate volume, was thus rejected (**Paper III**). If this difference is not accounted for, a reduction in the treated prostate volume could occur in an implementation of an MRI-only workflow.

Treatment planning using the vendor-independent MriPlanner sCT-generation software was found to be robust for equipment from a variety of MRI systems, at different field strengths and using different treatment techniques (**Paper IV**). Small dose differences were found compared to CT-based treatment planning. This paves the way for the widespread implementation of MRI-only workflows. CBCT images can be used for gross error detection in the sCT images, allowing CT imaging to be completely

eliminated from the workflow (**Paper V**), and CBCT images have the potential to verify the positions of gold fiducial markers. In conclusion, the work presented in this thesis demonstrates that an MRI-only workflow for radiotherapy of prostate cancer can be clinically implemented.

6 Future perspectives

The standardization of methods in MRI-only workflows is difficult due to the wide variety of sCT-generation methods and the different ways in which they have been incorporated into clinical workflows. Nevertheless, standardization is not only a concern for MRI-only workflows, but applies to radiotherapy in general. Professional organizations, such as the American Association of Physicists in Medicine, the European Society for Radiotherapy and the International Atomic Energy Agency, have, despite great variety, published guidelines and recommendations on other topics. Some of the questions related to MRI simulation in radiotherapy are addressed in the task group No. 284 of the American Association of Physicists in Medicine. MRI-only workflows for prostate cancer would benefit from guidelines. This would promote the implementation of MRI-only workflows in clinical practice.

The most important advantages of MRI-only workflows have been reported to be reduced uncertainties, time saving and cost efficacy. Health-economic studies are required to estimate the potential cost efficacy of MRI-only workflows. During the transition from dual-modality workflows to MRI-only workflows, new QA procedures will be necessary, which may lead to increased costs. The implementation of the sCT-generation method will also lead to increased costs, as software must be purchased from a vendor or developed in-house. These extra costs mean that MRI-only workflows may not be as cost efficient as initially expected. In order to be cost efficient, the costs of the extra QA-procedures and sCT-software, should not exceed the cost of a CT-appointment. Apart from the possible economic advantages of an MRI-only workflow, health aspects must be considered. A reduction in image registration uncertainties enables smaller PTV margins, potentially resulting in reduced toxicity. This could mean fewer healthcare visits from patients, since they experiences less side effects from their treatments, which would be a health economic benefit to society. This would be an interesting addition to the health economical calculation.

During recent years, there has been an increased interest in the application of artificial intelligence in healthcare, including the radiotherapy community. An example of its use is the development of deep-learning methods for sCT generation. Deep-learning offers faster sCT generation, which is especially interesting in the case of the MR-linac.

The MR-linac is based on CT images and deformable image registration, and thus potential image registration uncertainty. An MRI-only workflow could be used in the MR-linac, and would eliminate the need for CT imaging in this treatment modality. In the MR-linac, the sCT images are required in real time, which places high demands on the generation speed. Artificial intelligence could also be used in the development of automatic QA procedures, such as the CBCT-QA suggested in this thesis, which would benefit from being fully automated.

Radiotherapy of prostate cancer has recently seen a development towards more individualized treatment, including highly conformal treatment techniques and steep dose gradients. There is also a trend towards higher fractionation doses, fewer treatments and integrated boosts to parts of the target. This places high demands on the accuracy and precision of the radiotherapy workflow, and its underlying image information. Boost doses to parts of the target measuring a few mm may be associated with risks if the uncertainty in image registration in the workflow is of the same order of magnitude. MR-positron emission tomography (PET), which offers excellent soft tissue visualization and metabolic uptake information, is a modality with interesting potential in radiotherapy. Development of sCT-generation methods for attenuation correction in MR-PET is an ongoing research field that does not involve radiotherapy. Combining an MRI-only workflow with MR-PET into an MR-PET-only workflow is an interesting area of research for further development of personalized radiotherapy.

This thesis describes the development and implementation of an MRI-only workflow for radiotherapy of prostate cancer. The motivations, as well as the challenges, have been discussed. Patients with other forms of cancer, such as brain, head-and-neck and other abdominal cancers, may also benefit from an MRI-only workflow. Other challenges may arise in the workflows for these diagnoses, and solutions other than those presented in this thesis may be necessary.

7 Acknowledgements

Over the past years many people have contributed to the work presented in this thesis in one way or another. I am very grateful to all of them, but some deserve special thanks.

First of all, I would like to thank my main scientific supervisor, **Lars E Olsson**, for his guidance along the winding road that led to this thesis. Thank you for always believing in me, even when I didn't.

My scientific supervisor **Sofie Ceberg**, for her never-ending enthusiasm and encouragement. I am eternally grateful to you for taking time from your own work to support me in all matters.

My scientific supervisor **Adalsteinn Gunnlaugsson**, for his guidance in the world of oncology and prostate cancer treatment. Thank you for always taking the time to answer my questions, and for sharing your knowledge in both research and clinical work.

All former and present colleagues at the Department of Oncology and Radiation Physics in Lund and the Department of Medical Radiation Physics in Malmö. A special thanks to **Christian Jamtheim Gustafsson**, my constant MR-guide and friend; this journey would not have been as enjoyable, or even possible, without your support and our team work; to **Minna Lerner**, for her friendship and abundant good advice during our years of studying and working together; and to **Patrik Brynolfsson**, for his never-ending enthusiasm, knowledge and kind help with everything.

Thanks also to **Sven Bäck** and **Per Munck af Rosenschöld**, for giving me the opportunity to combine clinical work and research, and for always supporting me in the best possible way.

Thanks to **Andrej Tomaszewicz** and **Sacha af Wetterstedt,** for arranging my clinical work and answering all my questions regarding clinical practicalities.

Fredrik Nordström, who introduced me to the world of research during my work on my Master's dissertation. Thank you for your guidance, for always challenging me with your critical eye, and for all your ideas.

Joakim Jonsson, thank you for your guidance in the MRI-only world, and for all the enjoyable times during collaborations and travelling. Whether officially in the records or not, I will always consider you as one of my scientific supervisors.

Special thanks to all the clinical staff for their excellent help during these studies. Your knowledge and input made important contributions to the work presented here. Special thanks also to the MRI technicians **Senada Kapetanovic**, **Sveinung Groven**, **Anna Lippe** and **Urban Alkhed**, for your contributions to these studies, not least the observer study.

My friends and colleagues in **Umeå** and **Göteborg**, thank you for welcoming me to your departments, for good collaboration and for being splendid travel companions at many conferences.

I would also like to thank **Carl Siversson** and the **Spectronic Medical** staff, for fruitful collaboration, the supply of the software and their support throughout this work.

To the **Swedish VINNOVA Gentle Radiotherapy** consortium and all its collaborating hospitals, universities and companies: it has been a true privilege to be involved in this project.

Till min familj – Denna avhandling hade verkligen inte blivit till utan er. **Mamma** och **Pappa**, ni har alltid trott på mig, oavsett vad jag gett mig in på, och uppmuntrat mig att följa min egen väg. Mina systrar, **Karolina** och **Rebecka**, tack för ert stöd genom åren av studier och för att ni förgyller vardagen. **Adelen** och **Adrian**, moster älskar er. Oavsett vad ni bestämmer er för att göra i era liv är jag säker på att ni kommer åstadkomma underverk.

Mest av allt vill jag tacka **Johan**, min älskade livskamrat, som alltid är där för mig. Jag hade inte klarat detta utan dig vid min sida. Du gör mig otroligt lycklig, du är helt enkelt bäst.

This work was supported by:

- VINNOVA, Gentle Radiotherapy project (2016-03847 and 2016-02529)
- Allmänna sjukhusets i Malmö Stiftelse för bekämpande av cancer
- Stiftelsen för cancerforskning vid Onkologiska kliniken vid Universitets-sjukhuset MAS
- Skåne University Hospital, Lund, Sweden
- John and Augusta Persson's Foundation for Medical Research

8 References

Adjeiwaah, M., Bylund, M., Lundman, J. A., Karlsson, C. T., Jonsson, J. H. & Nyholm, T. 2018. Quantifying the Effect of 3T Magnetic Resonance Imaging Residual System Distortions and Patient-Induced Susceptibility Distortions on Radiation Therapy Treatment Planning for Prostate Cancer. *Int J Radiat Oncol Biol Phys,* 100, 317-324.

Arabi, H., Dowling, J. A., Burgos, N., Han, X., Greer, P. B., Koutsouvelis, N. & Zaidi, H. 2018. Comparative study of algorithms for synthetic CT generation from MRI: Consequences for MRI-guided radiation planning in the pelvic region. *Med Phys,* 45, 5218-5233.

Aramburu Nunez, D., Fontenla, S., Rydquist, L., Del Rosario, G., Han, Z., Chen, C. C., Mah, D. & Tyagi, N. 2020. Dosimetric evaluation of MR-derived synthetic-CTs for MR-only proton treatment planning. *Med Dosim*.

Ballhausen, H., Li, M., Hegemann, N. S., Ganswindt, U. & Belka, C. 2015. Intra-fraction motion of the prostate is a random walk. *Phys Med Biol,* 60, 549-63.

Bird, D., Henry, A. M., Sebag-Montefiore, D., Buckley, D. L., Al-Qaisieh, B. & Speight, R. 2019. A Systematic Review of the Clinical Implementation of Pelvic Magnetic Resonance Imaging-Only Planning for External Beam Radiation Therapy. *Int J Radiat Oncol Biol Phys,* 105, 479-492.

Bruynzeel, A. M. E., Tetar, S. U., Oei, S. S., Senan, S., Haasbeek, C. J. A., Spoelstra, F. O. B., Piet, A. H. M., Meijnen, P., Bakker Van Der Jagt, M. a. B., Fraikin, T., Slotman, B. J., Van Moorselaar, R. J. A. & Lagerwaard, F. J. 2019. A Prospective Single-Arm Phase 2 Study of Stereotactic Magnetic Resonance Guided Adaptive Radiation Therapy for Prostate Cancer: Early Toxicity Results. *Int J Radiat Oncol Biol Phys*.

Chen, L., Price, R. A., Jr., Wang, L., Li, J., Qin, L., Mcneeley, S., Ma, C. M., Freedman, G. M. & Pollack, A. 2004. MRI-based treatment planning for radiotherapy: dosimetric verification for prostate IMRT. *Int J Radiat Oncol Biol Phys,* 60, 636-47.

Chen, S., Qin, A., Zhou, D. & Yan, D. 2018. Technical Note: U-net-generated synthetic CT images for magnetic resonance imaging-only prostate intensity-modulated radiation therapy treatment planning. *Med Phys,* 45, 5659-5665.

Christiansen, R. L., Jensen, H. R. & Brink, C. 2017. Magnetic resonance only workflow and validation of dose calculations for radiotherapy of prostate cancer. *Acta Oncol,* 56, 787-791.

Cramer, A. K., Haile, A. G., Ognjenovic, S., Doshi, T. S., Reilly, W. M., Rubinstein, K. E., Nabavizadeh, N., Nguyen, T., Meng, L. Z., Fuss, M., Tanyi, J. A. & Hung, A. Y. 2013. Real-time prostate motion assessment: image-guidance and the temporal dependence of intra-fraction motion. *BMC Med Phys,* 13, 4.

Dawson, L. A., Litzenberg, D. W., Brock, K. K., Sanda, M., Sullivan, M., Sandler, H. M. & Balter, J. M. 2000. A comparison of ventilatory prostate movement in four treatment positions. *Int J Radiat Oncol Biol Phys,* 48, 319-23.

De Crevoisier, R., Bayar, M. A., Pommier, P., Muracciole, X., Pene, F., Dudouet, P., Latorzeff, I., Beckendorf, V., Bachaud, J. M., Laplanche, A., Supiot, S., Chauvet, B., Nguyen, T. D., Bossi, A., Crehange, G. & Lagrange, J. L. 2018. Daily Versus Weekly Prostate Cancer Image Guided Radiation Therapy: Phase 3 Multicenter Randomized Trial. *Int J Radiat Oncol Biol Phys,* 102, 1420-1429.

Debois, M., Oyen, R., Maes, F., Verswijvel, G., Gatti, G., Bosmans, H., Feron, M., Bellon, E., Kutcher, G., Van Poppel, H. & Vanuytsel, L. 1999. The contribution of magnetic resonance imaging to the three-dimensional treatment planning of localized prostate cancer. *Int J Radiat Oncol Biol Phys,* 45, 857-65.

Dinis Fernandes, C., Dinh, C. V., Steggerda, M. J., Ter Beek, L. C., Smolic, M., Van Buuren, L. D., Pos, F. J. & Van Der Heide, U. A. 2017. Prostate fiducial marker detection with the use of multi-parametric magnetic resonance imaging. *Physics and Imaging in Radiation Oncology,* 1, 14-20.

Doemer, A., Chetty, I. J., Glide-Hurst, C., Nurushev, T., Hearshen, D., Pantelic, M., Traughber, M., Kim, J., Levin, K., Elshaikh, M. A., Walker, E. & Movsas, B. 2015. Evaluating organ delineation, dose calculation and daily localization in an open-MRI simulation workflow for prostate cancer patients. *Radiat Oncol,* 10, 37.

Dowling, J. A., Sun, J., Pichler, P., Rivest-Henault, D., Ghose, S., Richardson, H., Wratten, C., Martin, J., Arm, J., Best, L., Chandra, S. S., Fripp, J., Menk, F. W. & Greer, P. B. 2015. Automatic Substitute Computed Tomography Generation and Contouring for Magnetic Resonance Imaging (MRI)-Alone External Beam Radiation Therapy From Standard MRI Sequences. *Int J Radiat Oncol Biol Phys,* 93, 1144-53.

Edmund, J. M., Andreasen, D., Mahmood, F. & Van Leemput, K. 2015. Cone beam computed tomography guided treatment delivery and planning verification for magnetic resonance imaging only radiotherapy of the brain. *Acta Oncol,* 54, 1496-500.

Edmund, J. M. & Nyholm, T. 2017. A review of substitute CT generation for MRI-only radiation therapy. *Radiat Oncol,* 12, 28.

Fransson, A., Andreo, P. & Potter, R. 2001. Aspects of MR image distortions in radiotherapy treatment planning. *Strahlenther Onkol,* 177, 59-73.

Fu, J., Yang, Y., Singhrao, K., Ruan, D., Chu, F. I., Low, D. A. & Lewis, J. H. 2019. Deep learning approaches using 2D and 3D convolutional neural networks for generating male pelvic synthetic computed tomography from magnetic resonance imaging. *Med Phys,* 46, 3788-3798.

Ghadjar, P., Fiorino, C., Munck Af Rosenschold, P., Pinkawa, M., Zilli, T. & Van Der Heide, U. A. 2019. ESTRO ACROP consensus guideline on the use of image guided radiation therapy for localized prostate cancer. *Radiother Oncol*.

Ghose, S., Mitra, J., Rivest-Henault, D., Fazlollahi, A., Stanwell, P., Pichler, P., Sun, J., Fripp, J., Greer, P. B. & Dowling, J. A. 2016. MRI-alone radiation therapy planning for prostate cancer: Automatic fiducial marker detection. *Med Phys,* 43**,** 2218.

Gladwish, A., Pang, G., Cheung, P., D'alimonte, L., Deabreu, A. & Loblaw, A. 2014. Prostatic displacement during extreme hypofractionated radiotherapy using volumetric modulated arc therapy (VMAT). *Radiat Oncol,* 9**,** 262.

Greer, P., Martin, J., Sidhom, M., Hunter, P., Pichler, P., Choi, J. H., Best, L., Smart, J., Young, T., Jameson, M., Afinidad, T., Wratten, C., Denham, J., Holloway, L., Sridharan, S., Rai, R., Liney, G., Raniga, P. & Dowling, J. 2019. A Multi-center Prospective Study for Implementation of an MRI-Only Prostate Treatment Planning Workflow. *Front Oncol,* 9**,** 826.

Greer, P. B., Dowling, J. A., Lambert, J. A., Fripp, J., Parker, J., Denham, J. W., Wratten, C., Capp, A. & Salvado, O. 2011. A magnetic resonance imaging-based workflow for planning radiation therapy for prostate cancer. *Med J Aust,* 194**,** S24-7.

Gustafsson, C., Korhonen, J., Persson, E., Gunnlaugsson, A., Nyholm, T. & Olsson, L. E. 2017a. Registration free automatic identification of gold fiducial markers in MRI target delineation images for prostate radiotherapy. *Med Phys,* 44**,** 5563-5574.

Gustafsson, C., Nordstrom, F., Persson, E., Brynolfsson, J. & Olsson, L. E. 2017b. Assessment of dosimetric impact of system specific geometric distortion in an MRI only based radiotherapy workflow for prostate. *Phys Med Biol,* 62**,** 2976-2989.

Gustafsson, C., Persson, E., Gunnlaugsson, A. & Olsson, L. E. 2018. Using C-Arm X-ray images from marker insertion to confirm the gold fiducial marker identification in an MRI-only prostate radiotherapy workflow. *J Appl Clin Med Phys*.

Han, X. 2017. MR-based synthetic CT generation using a deep convolutional neural network method. *Med Phys,* 44**,** 1408-1419.

Hentschel, B., Oehler, W., Strauss, D., Ulrich, A. & Malich, A. 2011. Definition of the CTV prostate in CT and MRI by using CT-MRI image fusion in IMRT planning for prostate cancer. *Strahlenther Onkol,* 187**,** 183-90.

Huisman, H. J., Futterer, J. J., Van Lin, E. N., Welmers, A., Scheenen, T. W., Van Dalen, J. A., Visser, A. G., Witjes, J. A. & Barentsz, J. O. 2005. Prostate cancer: precision of integrating functional MR imaging with radiation therapy treatment by using fiducial gold markers. *Radiology,* 236**,** 311-7.

Iaea 2005. Quality assurance of external beam radiotherapy. *Radiation oncology physics: A handbook for teachers and students.* Vienna.

Iaea 2016. Accuracy requirements and uncertainties in radiotherapy. *IAEA human health series no.31.* Vienna.

Icru 1993. Prescribing, recording and reporting photon beam therapy. *ICRU report 50.*

Johnstone, E., Wyatt, J. J., Henry, A. M., Short, S. C., Sebag-Montefiore, D., Murray, L., Kelly, C. G., Mccallum, H. M. & Speight, R. 2018. Systematic Review of Synthetic Computed Tomography Generation Methodologies for Use in Magnetic Resonance Imaging-Only Radiation Therapy. *Int J Radiat Oncol Biol Phys,* 100, 199-217.

Jonsson, J., Nyholm, T. & Soderkvist, K. 2019. The rationale for MR-only treatment planning for external radiotherapy. *Clin Transl Radiat Oncol,* 18, 60-65.

Jonsson, J. H., Johansson, A., Soderstrom, K., Asklund, T. & Nyholm, T. 2013. Treatment planning of intracranial targets on MRI derived substitute CT data. *Radiother Oncol,* 108, 118-22.

Kapanen, M. & Tenhunen, M. 2013. T1/T2*-weighted MRI provides clinically relevant pseudo-CT density data for the pelvic bones in MRI-only based radiotherapy treatment planning. *Acta Oncol,* 52, 612-8.

Kemppainen, R., Suilamo, S., Tuokkola, T., Lindholm, P., Deppe, M. H. & Keyrilainen, J. 2017. Magnetic resonance-only simulation and dose calculation in external beam radiation therapy: a feasibility study for pelvic cancers. *Acta Oncol,* 56, 792-798.

Kemppainen, R., Vaara, T., Joensuu, T. & Kiljunen, T. 2018. Accuracy and precision of patient positioning for pelvic MR-only radiation therapy using digitally reconstructed radiographs. *Phys Med Biol,* 63, 055009.

Kerkmeijer, L. G. W., Maspero, M., Meijer, G. J., Van Der Voort Van Zyp, J. R. N., De Boer, H. C. J. & Van Den Berg, C. a. T. 2018. Magnetic Resonance Imaging only Workflow for Radiotherapy Simulation and Planning in Prostate Cancer. *Clin Oncol (R Coll Radiol),* 30, 692-701.

Kim, J., Miller, B., Siddiqui, M. S., Movsas, B. & Glide-Hurst, C. 2019. FMEA of MR-Only Treatment Planning in the Pelvis. *Adv Radiat Oncol,* 4, 168-176.

Knöös, T., Nilsson, M. & Ahlgren, L. 1986. A method for conversion of Hounsfield number to electron density and prediction of macroscopic pair production cross-sections. *Radiotherapy and Oncology,* 5, 337-345.

Korhonen, J., Kapanen, M., Keyrilainen, J., Seppala, T. & Tenhunen, M. 2014. A dual model HU conversion from MRI intensity values within and outside of bone segment for MRI-based radiotherapy treatment planning of prostate cancer. *Med Phys,* 41, 011704.

Korhonen, J., Kapanen, M., Sonke, J. J., Wee, L., Salli, E., Keyrilainen, J., Seppala, T. & Tenhunen, M. 2015. Feasibility of MRI-based reference images for image-guided radiotherapy of the pelvis with either cone-beam computed tomography or planar localization images. *Acta Oncol,* 54, 889-95.

Korsager, A. S., Carl, J. & Riis Ostergaard, L. 2016. Comparison of manual and automatic MR-CT registration for radiotherapy of prostate cancer. *J Appl Clin Med Phys,* 17, 294-303.

Kugele, M., Mannerberg, A., Norring Bekke, S., Alkner, S., Berg, L., Mahmood, F., Thornberg, C., Edvardsson, A., Back, S. a. J., Behrens, C. F. & Ceberg, S. 2019. Surface guided radiotherapy (SGRT) improves breast cancer patient setup accuracy. *J Appl Clin Med Phys,* 20, 61-68.

Köhler, M., Vaara, T., Van Grootel, R., Hoogeveen, R., Kemppainen, R. & Renisch, S. 2015. MR-only simulation for radiotherapy planning -- Whitepaper: Philips MRCAT for prostate dose calculations using only MRI data.

Langen, K. M. & Jones, D. T. 2001. Organ motion and its management. *Int J Radiat Oncol Biol Phys,* 50, 265-78.

Lee, Y. K., Bollet, M., Charles-Edwards, G., Flower, M. A., Leach, M. O., Mcnair, H., Moore, E., Rowbottom, C. & Webb, S. 2003. Radiotherapy treatment planning of prostate cancer using magnetic resonance imaging alone. *Radiother Oncol,* 66, 203-16.

Maspero, M., Savenije, M. H. F., Dinkla, A. M., Seevinck, P. R., Intven, M. P. W., Jurgenliemk-Schulz, I. M., Kerkmeijer, L. G. W. & Van Den Berg, C. a. T. 2018. Dose evaluation of fast synthetic-CT generation using a generative adversarial network for general pelvis MR-only radiotherapy. *Phys Med Biol,* 63, 185001.

Maspero, M., Seevinck, P. R., Schubert, G., Hoesl, M. A., Van Asselen, B., Viergever, M. A., Lagendijk, J. J., Meijer, G. J. & Van Den Berg, C. A. 2017a. Quantification of confounding factors in MRI-based dose calculations as applied to prostate IMRT. *Phys Med Biol,* 62, 948-965.

Maspero, M., Van Den Berg, C. a. T., Zijlstra, F., Sikkes, G. G., De Boer, H. C. J., Meijer, G. J., Kerkmeijer, L. G. W., Viergever, M. A., Lagendijk, J. J. W. & Seevinck, P. R. 2017b. Evaluation of an automatic MR-based gold fiducial marker localisation method for MR-only prostate radiotherapy. *Phys Med Biol,* 62, 7981-8002.

Mclaughlin, P. W., Narayana, V., Kessler, M., Mcshan, D., Troyer, S., Marsh, L., Hixson, G. & Roberson, P. L. 2004. The use of mutual information in registration of CT and MRI datasets post permanent implant. *Brachytherapy,* 3, 61-70.

Milosevic, M., Voruganti, S., Blend, R., Alasti, H., Warde, P., Mclean, M., Catton, P., Catton, C. & Gospodarowicz, M. 1998. Magnetic resonance imaging (MRI) for localization of the prostatic apex: comparison to computed tomography (CT) and urethrography. *Radiother Oncol,* 47, 277-84.

Nederveen, A. J., Van Der Heide, U. A., Dehnad, H., Van Moorselaar, R. J., Hofman, P. & Lagendijk, J. J. 2002. Measurements and clinical consequences of prostate motion during a radiotherapy fraction. *Int J Radiat Oncol Biol Phys,* 53, 206-14.

Nyholm, T., Nyberg, M., Karlsson, M. G. & Karlsson, M. 2009. Systematisation of spatial uncertainties for comparison between a MR and a CT-based radiotherapy workflow for prostate treatments. *Radiat Oncol,* 4, 54.

Olsson, C. E., Jackson, A., Deasy, J. O. & Thor, M. 2018. A Systematic Post-QUANTEC Review of Tolerance Doses for Late Toxicity After Prostate Cancer Radiation Therapy. *Int J Radiat Oncol Biol Phys,* 102, 1514-1532.

Parker, C. C., Damyanovich, A., Haycocks, T., Haider, M., Bayley, A. & Catton, C. N. 2003. Magnetic resonance imaging in the radiation treatment planning of localized prostate cancer using intra-prostatic fiducial markers for computed tomography co-registration. *Radiother Oncol,* 66, 217-24.

Persson, E., Ambolt, P., Gustafsson, C., Gunnlaugsson, A., Bäck, S., Engelholm, S. & Olsson, L. E. Clinical implementation of MR-only prostate radiotherapy excluding CT. ESTRO 37, 20-24 April 2018a Barcelona, Spain. Elsevier 2018 (Radiotherapy and Oncology).

Persson, E., Gustafsson, C., Jonsson, J., Ceberg, S., Gunnlaugsson, A. & Olsson, L. E. MR-driven radiotherapy of prostate cancer patients – a need for speed. AAPM, 2018b Nashwille, USA. Medical Physics: Wiley.

Persson, E., Jamtheim Gustafsson, C., Ambolt, P., Engelholm, S., Ceberg, S., Back, S., Olsson, L. E. & Gunnlaugsson, A. 2020. MR-PROTECT: Clinical feasibility of a prostate MRI-only radiotherapy treatment workflow and investigation of acceptance criteria. *Radiat Oncol,* 15, 77.

Port, J. D. & Pomper, M. G. 2000. Quantification and minimization of magnetic susceptibility artifacts on GRE images. *J Comput Assist Tomogr,* 24, 958-64.

Rasch, C., Barillot, I., Remeijer, P., Touw, A., Van Herk, M. & Lebesque, J. V. 1999. Definition of the prostate in CT and MRI: a multi-observer study. *Int J Radiat Oncol Biol Phys,* 43, 57-66.

Roberson, P. L., Mclaughlin, P. W., Narayana, V., Troyer, S., Hixson, G. V. & Kessler, M. L. 2005. Use and uncertainties of mutual information for computed tomography/magnetic resonance (CT/MR) registration post permanent implant of the prostate. *Med Phys,* 32, 473-82.

Salembier, C., Villeirs, G., De Bari, B., Hoskin, P., Pieters, B. R., Van Vulpen, M., Khoo, V., Henry, A., Bossi, A., De Meerleer, G. & Fonteyne, V. 2018. ESTRO ACROP consensus guideline on CT- and MRI-based target volume delineation for primary radiation therapy of localized prostate cancer. *Radiother Oncol,* 127, 49-61.

Schad, L. R., Bluml, S., Hawighorst, H., Wenz, F. & Lorenz, W. J. 1994. Radiosurgical treatment planning of brain metastases based on a fast, three-dimensional MR imaging technique. *Magn Reson Imaging,* 12, 811-9.

Schieda, N., Avruch, L., Shabana, W. M. & Malone, S. C. 2015. Multi-echo gradient recalled echo imaging of the pelvis for improved depiction of brachytherapy seeds and fiducial markers facilitating radiotherapy planning and treatment of prostatic carcinoma. *J Magn Reson Imaging,* 41, 715-20.

Schmidt, M. A. & Payne, G. S. 2015. Radiotherapy planning using MRI. *Phys Med Biol,* 60, R323-61.

Segedin, B. & Petric, P. 2016. Uncertainties in target volume delineation in radiotherapy - are they relevant and what can we do about them? *Radiol Oncol,* 50, 254-62.

Seppala, T., Visapaa, H., Collan, J., Kapanen, M., Beule, A., Kouri, M., Tenhunen, M. & Saarilahti, K. 2015. Converting from CT- to MRI-only-based target definition in radiotherapy of localized prostate cancer: A comparison between two modalities. *Strahlenther Onkol,* 191, 862-8.

Siversson, C., Nordstrom, F., Nilsson, T., Nyholm, T., Jonsson, J., Gunnlaugsson, A. & Olsson, L. E. 2015. Technical Note: MRI only prostate radiotherapy planning using the statistical decomposition algorithm. *Med Phys,* 42, 6090-7.

Smith, W. L., Lewis, C., Bauman, G., Rodrigues, G., D'souza, D., Ash, R., Ho, D., Venkatesan, V., Downey, D. & Fenster, A. 2007. Prostate volume contouring: a 3D analysis of segmentation using 3DTRUS, CT, and MR. *Int J Radiat Oncol Biol Phys,* 67, 1238-47.

Stroom, J. C., Kroonwijk, M., Pasma, K. L., Koper, P. C., Van Dieren, E. B. & Heijmen, B. J. 2000. Detection of internal organ movement in prostate cancer patients using portal images. *Med Phys,* 27, 452-61.

Sun, J., Dowling, J. A., Pichler, P., Parker, J., Martin, J., Stanwell, P., Arm, J., Menk, F. & Greer, P. B. 2015. Investigation on the performance of dedicated radiotherapy positioning devices for MR scanning for prostate planning. *J Appl Clin Med Phys,* 16, 4848.

Tenhunen, M., Korhonen, J., Kapanen, M., Seppala, T., Koivula, L., Collan, J., Saarilahti, K. & Visapaa, H. 2018. MRI-only based radiation therapy of prostate cancer: workflow and early clinical experience. *Acta Oncol,* 57, 902-907.

Tyagi, N., Fontenla, S., Zelefsky, M., Chong-Ton, M., Ostergren, K., Shah, N., Warner, L., Kadbi, M., Mechalakos, J. & Hunt, M. 2017a. Clinical workflow for MR-only simulation and planning in prostate. *Radiat Oncol,* 12, 119.

Tyagi, N., Fontenla, S., Zhang, J., Cloutier, M., Kadbi, M., Mechalakos, J., Zelefsky, M., Deasy, J. & Hunt, M. 2017b. Dosimetric and workflow evaluation of first commercial synthetic CT software for clinical use in pelvis. *Phys Med Biol,* 62, 2961-2975.

Tzikas, A., Karaiskos, P., Papanikolaou, N., Sandilos, P., Koutsouveli, E., Lavdas, E., Scarleas, C., Dardoufas, K., Lind, B. K. & Mavroidis, P. 2011. Investigating the clinical aspects of using CT vs. CT-MRI images during organ delineation and treatment planning in prostate cancer radiotherapy. *Technol Cancer Res Treat,* 10, 231-42.

Van Herk, M. 2004. Errors and margins in radiotherapy. *Semin Radiat Oncol,* 14, 52-64.

Van Herk, M., Remeijer, P., Rasch, C. & Lebesque, J. V. 2000. The probability of correct target dosage: dose-population histograms for deriving treatment margins in radiotherapy. *Int J Radiat Oncol Biol Phys,* 47, 1121-35.

Wang, D., Strugnell, W., Cowin, G., Doddrell, D. M. & Slaughter, R. 2004. Geometric distortion in clinical MRI systems Part II: correction using a 3D phantom. *Magn Reson Imaging,* 22, 1223-32.

Wegener, D., Zips, D., Thorwarth, D., Weiss, J., Othman, A. E., Grosse, U., Notohamiprodjo, M., Nikolaou, K. & Muller, A. C. 2019. Precision of T2 TSE MRI-CT-image fusions based on gold fiducials and repetitive T2 TSE MRI-MRI-fusions for adaptive IGRT of prostate cancer by using phantom and patient data. *Acta Oncol,* 58, 88-94.

Verhey, L. J. 1995. Immobilizing and Positioning Patients for Radiotherapy. *Semin Radiat Oncol,* 5, 100-114.

Vidakovic, S., Jans, H. S., Alexander, A. & Sloboda, R. S. 2006. Post-implant computed tomography-magnetic resonance prostate image registration using feature line parallelization and normalized mutual information. *J Appl Clin Med Phys,* 8, 21-32.

Widmark, A., Gunnlaugsson, A., Beckman, L., Thellenberg-Karlsson, C., Hoyer, M., Lagerlund, M., Kindblom, J., Ginman, C., Johansson, B., Bjornlinger, K., Seke, M., Agrup, M., Fransson, P., Tavelin, B., Norman, D., Zackrisson, B., Anderson, H., Kjellen, E., Franzen, L. & Nilsson, P. 2019. Ultra-hypofractionated versus conventionally fractionated radiotherapy for prostate cancer: 5-year outcomes of the HYPO-RT-PC randomised, non-inferiority, phase 3 trial. *Lancet,* 394, 385-395.

Wyatt, J. J., Brooks, R. L., Ainslie, D., Wilkins, E., Raven, E., Pilling, K., Pearson, R. A. & Mccallum, H. M. 2019. The accuracy of magnetic resonance - cone beam computed tomography soft-tissue matching for prostate radiotherapy *Physics and Imaging in Radiation Oncology,* 12, 49-55.

Yartsev, S. & Bauman, G. 2016. Target margins in radiotherapy of prostate cancer. *Br J Radiol,* 89, 20160312.

Zangger, K. & Armitage, L. M. 1999. Silver and gold NMR. *Met Based Drugs,* 6, 239-45.